
FUNCTIONAL CONNECTIVITY IN VISUAL AREAS FROM TOTAL CORRELATION

Qiang Li

Image Processing Laboratory
University of Valencia
Valencia, 46980
qiang.li@uv.es

Greg Ver Steeg

Information Sciences Institute
University of Southern California
Marina del Rey, CA 90292
gregv@isi.edu

Jesus Malo

Image Processing Laboratory
University of Valencia
Valencia, 46980
jesus.malo@uv.es

ABSTRACT

A recent study invoked the superiority of the *Total Correlation* concept over the conventional pairwise measures of functional connectivity in neuroscience. That seminal work was restricted to show that empirical measures of *Total Correlation* lead to connectivity patterns that differ from what is obtained using *linear correlation* and *Mutual Information*. However, beyond the obvious multivariate versus bivariate definitions, no theoretical insight on the benefits of Total Correlation was given. The accuracy of the empirical estimators could not be addressed because no controlled scenario with known analytical result was considered either.

In this work we analytically illustrate the advantages of *Total Correlation* to describe the functional connectivity in the visual pathway. Our neural model includes three layers (retina, LGN, and V1 cortex) and one can control the connectivity among the nodes, within the cortex, and the eventual top-down feedback. In this multivariate setting (three nodes with multidimensional signals), we derive analytical results for the three-way *Total Correlation* and for all possible pairwise *Mutual Information* measures. These analytical results show that pairwise *Mutual Information* cannot capture the effect of different intra-cortical inhibitory connections while the three-way *Total Correlation* can. The presented analytical setting is also useful to check empirical estimators of *Total Correlation*. Therefore, once certain estimator can be trusted, one can explore the behavior with natural signals where the analytical results (that assume Gaussian signals) are no longer valid. In this regard (a) we explore the effect of connectivity and feedback in the analytical retina-cortex network with natural images, and (b) we assess the functional connectivity in V1-V2-V3-V4 from actual fMRI recordings.

Keywords Functional Connectivity, Information in Networks, Total Correlation, Mutual Information, Visual Brain, Retina-Cortex Pathway, Linear Receptive Fields, Divisive Normalization, Intra-Cortical Connections.

1 Introduction

Functional connectivity in neural networks goes beyond structural links: it is related to the way information is shared among multiple neural nodes [1, 2]. Quantifying the communication between multiple neural regions is key to understand brain function. However, most of the literature on functional connectivity just describes pairwise relationships because the conventional measures (such as correlation and mutual information) cannot cope with more than two nodes simultaneously. As a result, studies involving more than two brain regions at the same time are rare.

A recent study proposed the use of Total Correlation as a way to overcome the intrinsic pairwise limitation of the conventional measures of functional connectivity in neuroscience [3]. The multivariate nature of Total Correlation, T [4] is a *by-definition* advantage over Mutual Information, I [5]. However, the seminal work that proposed T as a measure of functional connectivity [3] had a fundamental limitation: beyond the obvious multivariate definition of T , no extra theoretical insight on its benefits was given. As a result of the lack of analytical models, the accuracy of the empirical estimators could not be addressed because no controlled scenario was considered either.

The goal of this work is addressing the limitations of [3] in the context of the visual brain. We do it through the consideration of simple but plausible analytical models of the retina-V1-cortex pathway.

The three-node model considered here (retina-LGN-V1) consists of the conventional linear receptive fields plus Divisive Normalization nonlinearities [6–9]. Following [10, 11] we keep the dimensionality relatively small so that reliable estimations of information-theoretic variables can be done. However, the biological plausibility of the considered setting is explicitly checked against human data of visual psychophysics. In this general setting every node (or layer) has noisy neurons so that part of the visual information is lost along the way. We consider two variations of this theoretical setting: *Model I* is a nonlinear network with intra-cortical connections, and *Model II* is its linear version with top-down feedback. When considering Gaussian signals both *Model I* (nonlinear) and *Model II* (recurrent) are analytically tractable.

In this work we derive expressions for T and I depending on the feedforward and feedback structural connectivity. The key issue is the sensitivity of the descriptor: the bigger the variation of the descriptor in the range of explored connectivity the better. In that way, the representation of the connectivity will be more robust to errors in the estimation of the descriptor. Our analytical results show that while I is insensitive to some of the connectivity parameters, T is sensitive to the connectivity. These analytical results explicitly show the superiority of T over I as a description of the connectivity in a biologically plausible network.

On the other hand, the presented analytical results constitute a test-bed to check the accuracy of different empirical estimators for T (or I). In this way, available estimators (as for instance [12–17]) can be reliably applied to real data where theoretical results are not available (for instance because the Gaussian assumption is no longer valid [18–21]). Finally, in this paper we discuss the shared information between cortical areas using a recent fMRI dataset [22].

The structure of the paper is as follows. Section 2 describes the structural connectivity in the neural models considered throughout the work and their biological plausibility through the reproduction of visual psychophysics. In Section 3 we derive the analytical results for the functional connectivity (both I and T) in terms of the structural connectivity and the properties of the signal. In the analytical results we consider both feedforward nonlinear models and models with feedback. Section 4 presents T and I results computed with empirical estimators that can be compared to the theoretical results of Section 3. Moreover, results for real signals (natural images and actual responses measured using fMRI) are also presented here. Finally, Section 5 summarizes the results and discusses the implications of the work.

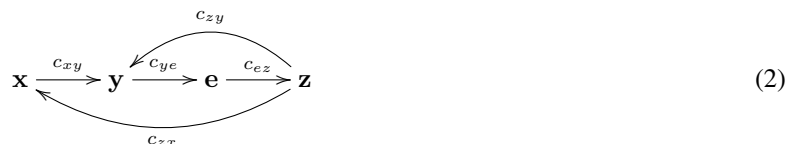
2 Models of the retina-cortex pathway

Expanding and making explicit the multi-node scenario first considered in [3], all the theoretical results of this work will be derived for the following *early vision* setting that may include feedforward and feedback connections, as for instance:



In this diagram the arrows represent structural connections between regions (or layers). Right-arrows represent feedforward flow of the visual information, and the left-arrows represent eventual feedback.

More specifically, the signal at the *retina* will be represented by the n -dimensional random vector, \mathbf{x} , the signal at the *LGN*, will be represented by the n -dimensional random vector, \mathbf{y} , and the signal at the cortex will be represented by two n -dimensional random vectors, \mathbf{e} and \mathbf{z} . In this way, the intra-cortical connectivity is represented by the communication between \mathbf{e} and \mathbf{z} . In the following diagram the strength of the structural connections between layers i and j is represented by the variables, c_{ij} :



In the above setting, the study of functional connectivity through information-theoretic measures (such as I or T) could be useful to describe the *unknown* strengths, c_{ij} , from recordings of the neural signal done at the different nodes or layers. In this context, proper measures of statistical relation should be sensitive to c_{ij} . And the bigger the sensitivity to the strength of the connections, the better.

2.1 *Model I*: Nonlinear and noisy model with focus on intra-cortical interactions

Our first specific example of the retina-cortex framework outlined in Eq. 2, which we will refer to as *Model I*, tries to be analytically simple yet biologically plausible. To do so, this model includes: (a) center-surround receptive fields in the LGN [23], (b) local-frequency receptive fields in the (linear) V1-cortex, approximated here as block-DCT basis functions [24, 25], (c) a Divisive Normalization transform to model cortical nonlinearities [8], and (d) noise in each of the neural layers is scaled in a way compatible with the psychophysical results in [26] and the physiological model in [27].

In Section 2.4 we will see that the above elements (the considered layers and noise levels) are critical for the correlation with human opinion in visual psychophysics. In this regard, the intra-cortical connectivity in the Divisive Normalization transform is particularly relevant. Therefore, eventual measures of the statistical relation between neural nodes should be sensitive to this intra-cortical connectivity.

The class of networks under *Model I* follows these equations:

$$\begin{aligned}
 \mathbf{x}(t) &= \mathbf{s}(t) + \mathbf{n}_x(t) + \frac{c_{zx}}{c_{xy} c_{ye}} F^{-1} \cdot \mathbf{z}(t - \Delta t) \\
 \mathbf{y}(t) &= c_{xy} K \cdot \mathbf{x}(t) + \mathbf{n}_y(t) = c_{xy} F^{-1} \cdot \lambda_{CSF} \cdot F \cdot \mathbf{x}(t) + \mathbf{n}_y(t) \\
 \mathbf{e}(t) &= c_{ye} F \cdot \mathbf{y}(t) + \mathbf{n}_e(t) \\
 \mathbf{z}(t) &= f(\mathbf{e}(t)) = \text{sign}(\mathbf{e}(t)) \cdot \kappa \cdot \frac{|\mathbf{e}(t)|^\gamma}{b + c_{ez} H \cdot |\mathbf{e}(t)|^\gamma}
 \end{aligned} \tag{3}$$

where, the input to the system is the retinal image: the source vector $\mathbf{s} \in \mathbb{R}^n$, and its dimension n corresponds to the number of photoreceptors. In the models considered in this work, the networks preserve the dimension of the signal¹.

The retinal signal, the vector $\mathbf{x} \in \mathbb{R}^n$, is influenced by the input image \mathbf{s} , but it is also affected by the white noise \mathbf{n}_x and in this formulation, by a top-down feedback signal given by the term weighted by c_{zx} , that describes the strength of this feedback connection. Due to the eventual variations in the input and the eventual feedback, all the multivariate signals may depend on time, t . We will come back to the feedback term once we introduce the frequency meaning of vector \mathbf{z} .

The signal at the LGN is described by the vector $\mathbf{y} \in \mathbb{R}^n$. The matrix K contains the center-surround receptive fields of LGN [23]. According to the relation between these receptive fields and the Contrast Sensitivity Function (CSF) [30–32], we implement them using a local-frequency transform (basis in the matrix F), a diagonal matrix with CSF-related weights, λ_{CSF} , and coming back to the spatial domain using F^{-1} . The LGN signal is also affected by white noise through \mathbf{n}_y .

The (intermediate) linear signal at the V1-cortex, \mathbf{e} , is computed from the LGN signal through a set of local-frequency receptive fields in the matrix F . This linear signal is also affected by the white noise \mathbf{n}_e .

Finally, the nonlinear signal at V1, \mathbf{z} , results from a Divisive Normalization transform, $f(\cdot)$, of the outputs of the linear receptive fields at the previous intermediate layer, \mathbf{e} . Note that the division, the exponent, and the absolute values in $f(\cdot)$ are Hadamard (element-wise) operations [33], and the matrix H in the denominator represents the interaction between the neurons of the previous cortical layer \mathbf{e} . Specifically, the intra-cortical connectivity between the k -th and the l -th neurons is represented by $c_{ez} H_{kl}$. In this way, the k -th row of H , $H_{kl} \forall l = 1, \dots, n$, describes how the responses of the neighbor linear neurons, e_l , affect the nonlinear response of the k -th neuron, z_k . This interaction is assumed to be local in space and frequency [9, 33, 34]. And c_{ez} controls the global strength of all these local interactions.

Finally, a comment on the top-down feedback term in the first equation. The Divisive Normalization changes the relative magnitude of the responses z_i but the rough qualitative meaning of the responses in \mathbf{z} is still given by the (local-frequency) receptive fields in F . Therefore, the F^{-1} matrix in the top-down feedback term in the first equation of the system just converts the previous cortical response $\mathbf{z}(t - \Delta t)$ back into the spatial domain (where the input images \mathbf{s} are). Additionally, the top-down term has been scaled by the other connectivity strengths (c_{xy} and c_{ye}) just to keep the scale of the feedback term comparable to the source independently of the (arbitrary) gains introduced along the retina-cortex path. In this way the effective weight of the feedback term only depends on c_{zx} .

The parameters that control the feedforward structural connections between retina, LGN, and the linear V1, (i.e. the strengths c_{xy} and c_{ye}) actually control the size of the signal with regard to the noise, and hence their functional role is

¹Preservation of dimension along the pathway is convenient but it doesn't reduce the generality neither biologically, the spatial subsampling affects the extrafovea, but not the fovea [28], nor mathematically because changes of dimension could be addressed by the Jacobians of rectangular transforms [29].

quite evident: the bigger the signal compared to the noise, the stronger the information flow from one node/layer to the next. However, the role of the intra-cortical interaction $c_{ez}H$ is more interesting. There is a large body of literature that suggests that the role of the denominator in Divisive Normalization is capturing-and-removing the statistical relations between the responses of the linear local-frequency sensors [20, 21, 35–38].

The first set of analytical results derived in Section 3.1 shows how T is sensitive to this (eventually interesting) intra-cortical connectivity, while the sensitivity of I to these intra-cortical connections is equal to zero. This is an analytical example (for a biologically plausible nonlinear network) of the genuine superiority of the Total Correlation over the conventional Mutual Information.

2.2 *Model II*: Linear noisy model with focus on feedback

Model II is just a variation of *Model I* intended to simplify the analytical study of feedback. The convenience of this variation will become apparent in Section 3 when we derive the analytical results. By comparing the Eqs. 3 of *Model I* and Eqs. 4 of *Model II* it is easy to see that our second class of networks is just a linear version of the first where we disregarded the Divisive Normalization. Specifically, in the last equation of *Model II* the cortical nonlinearity $f(\cdot)$ has been substituted by a trivial identity, \mathbb{I} , and the input cortical signal is scaled by the strength c_{ez} with regard to the inner noise \mathbf{n}_z , which was not present before:

$$\begin{aligned} \mathbf{x}(t) &= \mathbf{s}(t) + \mathbf{n}_x(t) + \frac{c_{zx}}{c_{xy} c_{ye} c_{ez}} F^{-1} \cdot \mathbf{z}(t - \Delta t) \\ \mathbf{y}(t) &= c_{xy} K \cdot \mathbf{x}(t) + \mathbf{n}_y(t) = c_{xy} F^{-1} \cdot \lambda_{CSF} \cdot F \cdot \mathbf{x}(t) + \mathbf{n}_y(t) \\ \mathbf{e}(t) &= c_{ye} F \cdot \mathbf{y}(t) + \mathbf{n}_e(t) \\ \mathbf{z}(t) &= c_{ez} \mathbb{I} \cdot \mathbf{e}(t) + \mathbf{n}_z(t) \end{aligned} \quad (4)$$

Recurrence implied by feedback (both in *Model I* and *Model II*) implies a nontrivial evolution of the signals when the system faces dynamic inputs with fast variations compared with the updating time constant Δt . In this work we will restrict ourselves to slow-varying sources $\mathbf{s}(t)$ and we wait till the convergence of the signals to a stationary state to measure the statistical dependence between the signals at the different layers.

In the setting described by *Model II* the information about the input image (or source \mathbf{s}) flows through the feedforward links while being contaminated by the noise injected at each layer. However, for the slow-varying inputs described above, part of the source is injected back into the retinal signal. As a result, the scenario in *Model II* is convenient to analyze the joint effect of the strength of the feedforward links and the feedback links. For example, one may study the effect of the intra-cortical connectivity c_{ez} (that scales the signal wrt the inner noise) together with the strength of the feedback c_{zx} that reinforces the presence of the source at the retina. From a naive perspective, increasing c_{ez} and c_{zx} seems to lead to an increase of the Signal-to-Noise ratio in all the responses. Analytical results of information-theoretic descriptors can confirm or refute this intuition and provide a tool to understand a variety of situations.

The second set of analytical results derived in Section 2.2 show that while T strongly depends on the feedforward and feedback strengths c_{ez} and c_{zx} , the sensitivity of I is smaller. In this case, the sensitivity of I is just smaller (not zero) but the substantial difference in sensitivities (in a biologically plausible recurrent scenario) illustrates the conceptual superiority of T over the conventional I .

2.3 Model parameters: receptive fields, divisive normalization and responses

In this section we present and illustrate the range of parameters that we considered in Eqs. 3 and 4 of *Model I* and *Model II*.

First, note that throughout the work we consider that the input to our system are achromatic image patches of 8×8 pixels. This means that vectors \mathbf{s} , \mathbf{x} , \mathbf{y} , \mathbf{e} , and \mathbf{z} live in \mathbb{R}^{64} , and we consider layers (or nodes) with $n = 64$ neurons. Therefore, matrices K , F , λ_{CSF} , and H (that represent relations between neurons) are 64×64 matrices.

Figure 1 illustrates the parameters involved in the retina-to-LGN transform ($\mathbf{x} \rightarrow \mathbf{y}$) and in the LGN-to-cortex transform ($\mathbf{y} \rightarrow \mathbf{z}$), as well as in the intra-cortical nonlinearity ($\mathbf{e} \rightarrow \mathbf{z}$) of *Model I*.

First, regarding $\mathbf{x} \rightarrow \mathbf{y}$ we follow the relation between the center-surround cells in LGN and the CSF, and hence we compute K from the CSF of the Standard Spatial Observer [39] transformed from the original Fourier domain into the (more convenient) DCT domain using the procedure in [40] (second panel in Fig. 1). The result (in the spatial domain) are center-surround receptive fields which are consistent with the physiological measurements [23] (first panel in 1).

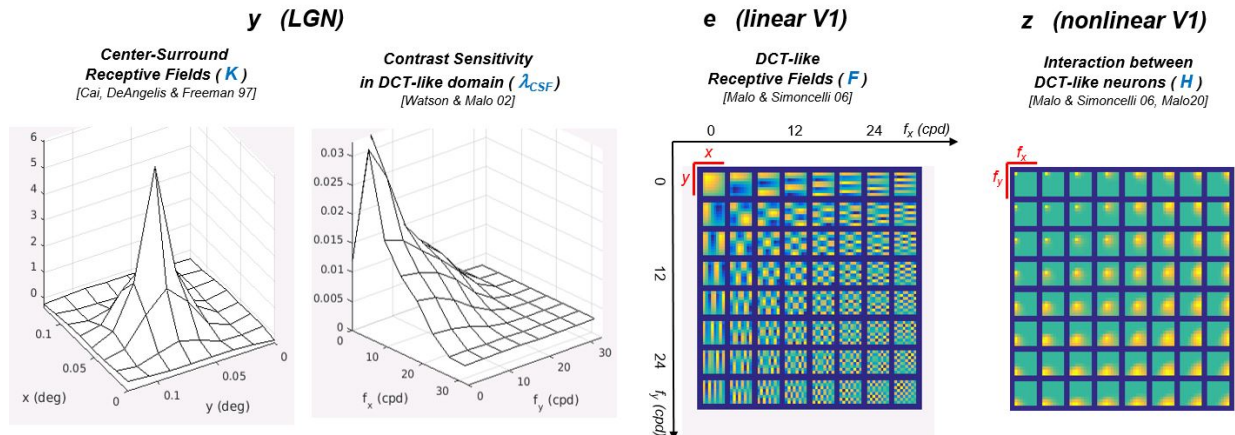


Figure 1: Center-surround receptive fields in LGN and equivalent Contrast Sensitivity Function. Local frequency filters tuned to different orientations in linear V1 and interaction kernel $H_{ff'}$ in the divisive normalization nonlinearity in V1.

Then, the linear cortical transform $\mathbf{y} \rightarrow \mathbf{e}$ uses the local-DCT representation following previous results on biologically-inspired image compression [41, 42] and subjective image quality [43, 44]. The 64×64 local-frequency receptive fields in F (DCT-like basis functions) are shown in the third panel of Fig. 1.

Finally, regarding the intra-cortical Divisive Normalization, $\mathbf{e} \rightarrow \mathbf{z}$, here we also follow models used in biologically-inspired image compression methods [37, 45]. In this case, the structural connectivity between different local-frequency sensors decays with distance in frequency according to a Gaussian [33, 34]:

$$H_{ff'} = e^{-\frac{(f-f')^2}{\sigma(f)^2}} \quad (5)$$

where the width $\sigma(f)$ increases with the frequency f , according to $\sigma(f) = \sigma_0 + \alpha_H f$, as illustrated in the example of the fourth panel of Fig. 1. In that case, the connectivity neighborhood is wider for sensors of high frequency (bottom right of the plot) than for sensors of low frequency (top left of the plot). Finally, in our experiments we set the semi-saturation constant b and the constant κ according to the method in [10] so that the Divisive Normalization is compatible with classical non-linearities such as the Wilson-Cowan recurrent model [46].

In the experiments we consider a range of intra-cortical connectivity values in *Model I* (section 3.1), and we modify the width of the kernel H by varying the constant $\alpha_H \in [0.35, 4]$, and by varying the strength $c_{ez} \in [0.01, 300]$. This has an effect in the nonlinearity of the cortical responses and, as a consequence, on the statistical effect of $f(\cdot)$.

Figure 2 illustrates the transformations of the signal along the layers of *Model I* for a representative set of parameters (those that maximize correlation with human psychophysics). The top panel shows (i) the input image \mathbf{s} : in this case the achromatic image of an eye in the range $[0, 200] \text{ cd/m}^2$, spatially sampled at 64 cycles/degree, (ii) how this input is distorted with the noise at the retina (leading to \mathbf{x}), (iii) the response of center-surround cells distorted by noise in \mathbf{y} , (iv) the response to 3×3 regions of local-frequency sensors in \mathbf{e} (with the corresponding noise) in \mathbf{e} , and finally, (v) the result of the Divisive Normalization in \mathbf{z} . Additionally, for a qualitative understanding of the information lost along the way, the cortical signals (\mathbf{e} and \mathbf{z}) are represented back in the spatial domain by transforming them using the linear inverse F^{-1} .

Following the argument in [26] the standard deviation of the noise injected at each layer has been selected such as it remains barely visible. This is because just-noticeable-differences are determined by this amount of noise [47]. Specifically, the standard deviation of the white noise at the different layers in *Model I* is $\sigma(n_x) = 5 \text{ cd/m}^2$ (for images with luminance in the range $[0, 200] \text{ cd/m}^2$), $\sigma(n_y) = 0.1$, $\sigma(n_e) = 0.01$, and (on top of these values), in *Model II* we have $\sigma(n_z) = 0.01$.

Finally, the scatter plots at the bottom left of Fig. 2 illustrate the nonlinearities introduced by the considered Divisive Normalization. From the local DC components of the representation we can see the saturation of (perceived) brightness as a function of the input luminance, where we can see the Weber Law [48]. Similarly, the other plots for *low*, *medium*, and *high*, frequency coefficients, illustrate the nonlinearity of the perceived contrast as a function of the input contrasts. This sigmoidal and signal-dependent behavior is consistent with the psychophysics of contrast perception [34], and the amplitude of the responses for the different frequencies is consistent with the CSF [32, 40].

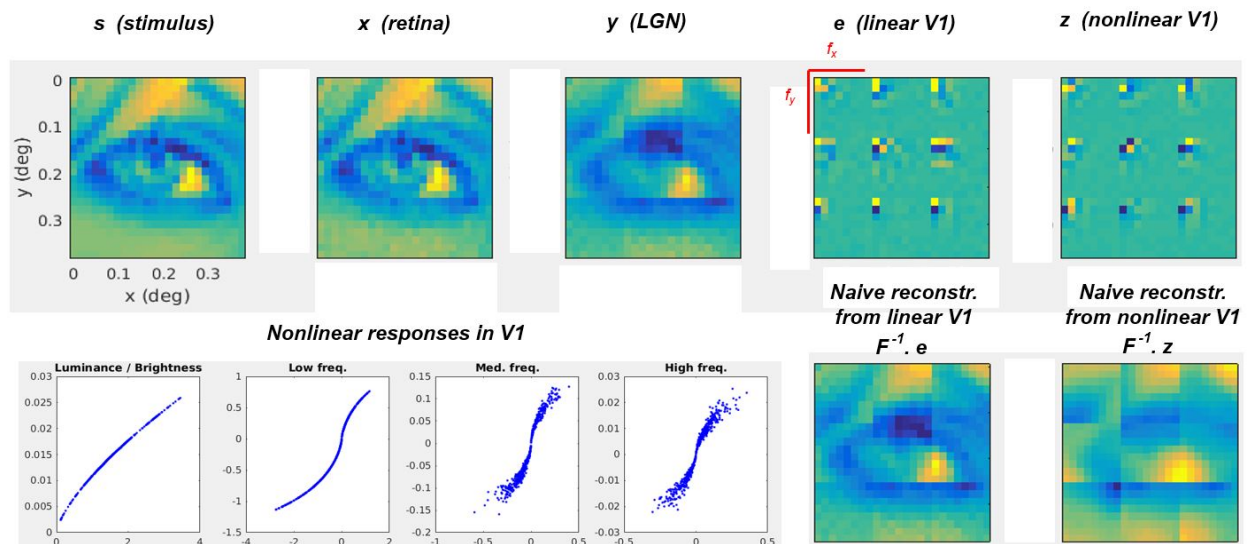


Figure 2: Responses to a sample image with the optimal set of parameters. Optimal means maximum correlation with human opinion among the considered discrete set of cortical connectivity values.

2.4 Model plausibility: image quality psychophysics

Qualitative Weber law, saturation of perceived contrast, and compatibility with the CSF displayed in Fig. 2 suggest that the parameters selected from the literature make sense. However, a more comprehensive/quantitative test is necessary particularly if a range of parameters has to be considered. To this end, in this section we assess the plausibility of the models according to their ability to predict experimental data on subjective image quality, specifically the ratings given by humans in the TID database [49]. This way of determining biologically plausible parameters is not new [21, 39, 50] and it has been subject to criticism as a single measurement of performance [9]. However, in the context presented here, prediction of subjective quality is enough to highlight the general behavior of the model and to (roughly) identify which regions of the parameter space make more biological sense.

In this regard, the scatter plots in Figure 3 show how well Euclidean distances at the different layers of *Model I* (abscissas), predict the subjective ratings (ordinates). The strong correlation obtained in the inner cortical representation $\rho = 0.84$, which is not far from the state-of-the-art in subjective image quality metrics [51] prove the plausibility of the transforms and the levels of the Gaussian noise introduced at each layer.

Specifically, the poor result for the input representation (s in luminance) implies that the visual brain certainly *does something else* to the input signal [52, 53]. The progressive improvement of the correlation along deeper layers means that the set of considered transforms is biologically meaningful. In fact, the consideration of the center-surround cells (or the CSF) is a major fact in explaining image quality [39, 43], and this is incorporated in both models leading to a reasonable Pearson correlation, $\rho = 0.71$, only with linear transforms. Then, we study the intra-cortical connectivity of *model I* in more detail: we consider the plausibility of a range of strengths c_{ez} and a range of widths in H .

The result shows that all the family of Divisive Normalization transforms make sense because they substantially improve the correlation with human opinion. Note that the correlation at the linear cortical layer e (surface in light blue at 0.71) is raised by the different z layers to be in the range $[0.76, 0.84]$. Moreover, the final correlation surface for the different intra-cortical connectivity values has strong curvature and a clear maximum (green dot) in the middle of the considered region. This means that it is interesting to study the behavior of the statistical descriptors of connectivity in this region of parameters.

3 Analytical results: T and I in terms of intra-layer connectivity and feedback

Here we present results for *Model I* and *Model II* which address different interesting situations that may happen in natural or artificial neural nets: (i) nonlinear intra-layer connectivity, and (ii) feedback or recurrence. In order to simplify the analytical tractability, in each case we focus on a specific feature of the models, either the nonlinearity (in *Model I*) or the feedback-recurrence (in *Model II*).

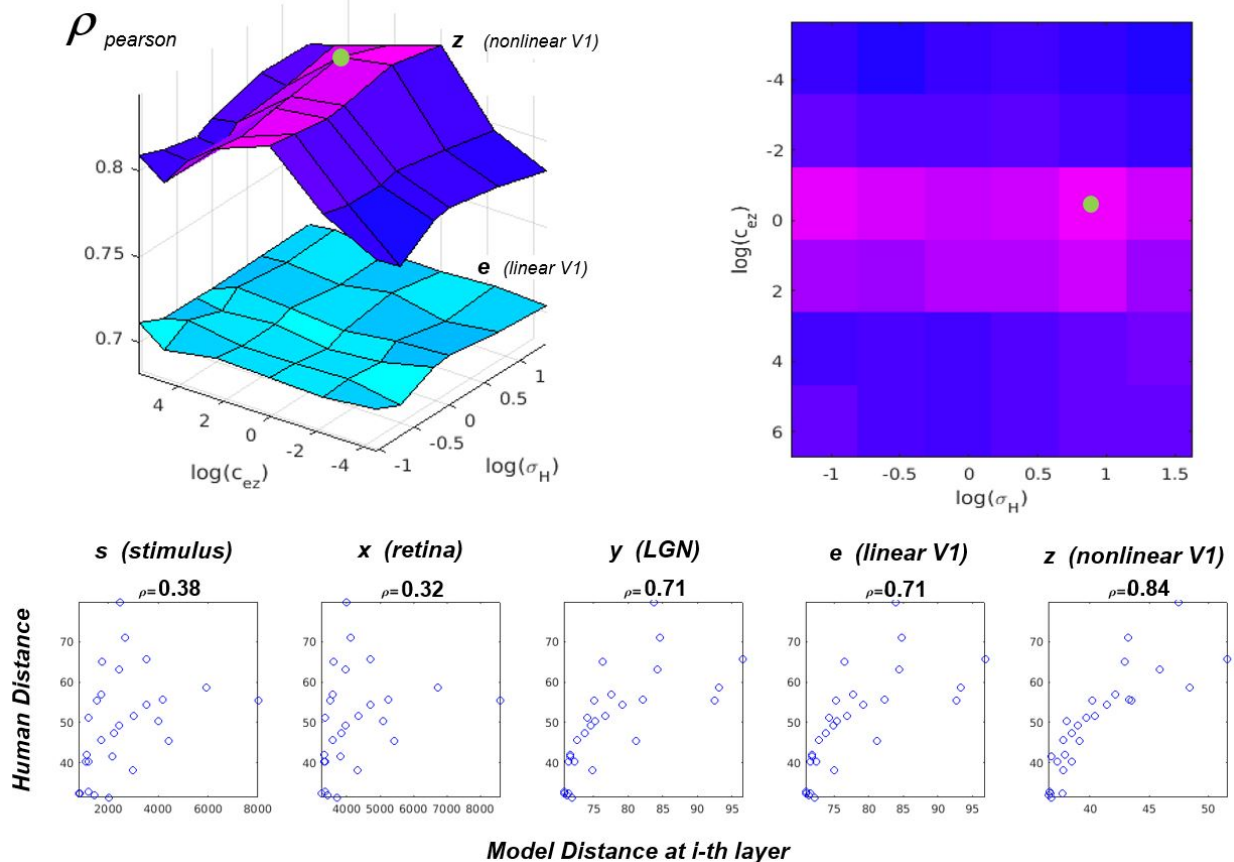


Figure 3: Correlation with human opinion for different cortical connectivity values (surfaces on top) and correlations in previous (linear) layers (scatter plots at the bottom). In the nonlinear cortical case the scatter plot is the one corresponding to the optimum connectivity.

For both models (*I* and *II*) analytical tractability is simple if one considers Gaussian signals. The Gaussian assumption for natural images has been acknowledged as a too rough approximation both in Visual Neuroscience [18–21] and in Image Processing [54, 55]. However, in this section we are going to take this assumption for the sake of analytical tractability. In the experimental section we will compare the results with (synthetic) Gaussian signals and natural inputs. The Gaussian assumption is appropriate and illustrative in this case because (as shown below using a trustable empirical estimator) results for natural images are (1) similar to the Gaussian results, and more important for this work, (2) they confirm the superiority of the description using T also for natural signals.

For the reader convenience, let's recall the definitions of the descriptors considered here: *Total Correlation* [4], and *Mutual Information* [5] in terms of *Entropy*:

$$T(\mathbf{x}, \mathbf{y}, \mathbf{z}) = \left(\sum_{i=1}^n h(x_i) + h(y_i) + h(z_i) \right) - h(\mathbf{x}, \mathbf{y}, \mathbf{z}) \quad (6)$$

$$I(\mathbf{x}, \mathbf{y}) = h(\mathbf{x}) + h(\mathbf{y}) - h(\mathbf{x}, \mathbf{y}) \quad (7)$$

The biggest conceptual difference between these magnitudes is, of course, that T can be applied to *any* number of nodes (or layers). However, even in the case of just two nodes, $T(\mathbf{x}, \mathbf{y}) \neq I(\mathbf{x}, \mathbf{y})$ because, for multivariate nodes, T considers the redundancy among the coefficients (or neurons) of each node, which is disregarded by I . This difference is key when the signals in each layer are not independent, which is the more interesting situation in visual neuroscience.

As joint and marginal entropy are easily computed for Gaussian signals from the covariance matrices or from the marginal variances [5], Eqs. 6 and 7 imply that, if variables are Gaussian, analytical results are straightforward. This is the case in *Model II*, but, due to the nonlinearity, it is not the case in *Model I*.

3.1 T and I as descriptors of intra-cortical connectivity (*Model I*)

For the sake of simplicity, in this section, on top of the Gaussian assumption mentioned above, we will also consider $c_{zx} = 0$ in our nonlinear *Model I*, i.e. it does not consider feedback. We leave feedback for the results of *Model II* in Section 3.2.

With these assumptions, the variables \mathbf{x} , \mathbf{y} , and \mathbf{e} are Gaussian because they are sum of linearly-transformed Gaussian variables plus white Gaussian noise. However, the Divisive Normalization nonlinearity $f(\cdot)$ implies that the variable \mathbf{z} is non-Gaussian. In this setting, expressions for T and I involving \mathbf{z} (where the intra-cortical connectivity is) require the application of specific properties of these magnitudes under transforms of the random variables.

The Total Correlation does depend on intra-cortical connectivity:

In order to get an analytical result for $T(\mathbf{x}, \mathbf{y}, \mathbf{z})$, lets concatenate the variables that represent the considered nodes into column vectors of dimension $3n$: $\mathbf{a} = [\mathbf{x}; \mathbf{y}; \mathbf{e}]$, and $\mathbf{a}' = [\mathbf{x}; \mathbf{y}; \mathbf{z}] = [\mathbf{x}; \mathbf{y}; f(\mathbf{e})]$, and consider,

$$\mathbf{a} \xrightarrow{\mathcal{F}} \mathbf{a}'$$

where we are interested in computing $T(\mathbf{a}')$. In this situation, one may use the following property of the variation of Total Correlation when the variables undergo a transformation \mathcal{F} [11, 56]:

$$\Delta T(\mathbf{a}, \mathbf{a}') = T(\mathbf{a}) - T(\mathbf{a}') = \sum_i^{3n} h(a_i) - \sum_i^{3n} h(a'_i) + \frac{1}{2} \mathbb{E}_{\mathbf{a}} \{ \log |\nabla_{\mathbf{a}} \mathcal{F}^\top \cdot \nabla_{\mathbf{a}} \mathcal{F}| \} \quad (8)$$

where $\mathbb{E}_{\mathbf{a}} \{ \cdot \}$ is the average over the samples \mathbf{a} . Then, taking into account that,

$$\nabla_{\mathbf{a}} \mathcal{F} = \begin{pmatrix} \mathbb{I} & 0 \\ 0 & \nabla_{\mathbf{e}} f \end{pmatrix}$$

and considering that $T(\mathbf{a}) = T(\mathbf{x}, \mathbf{y}, \mathbf{e})$ only depends on Gaussian variables and hence with known entropy in terms of the covariance matrix², we obtain the desired result (in *nats*):

$$T(\mathbf{x}, \mathbf{y}, \mathbf{z}) = \frac{1}{2} \sum_i^{3n} \log(\Sigma_{ii}^a) - \frac{1}{2} \log |\Sigma^a| - \frac{n}{2} - \frac{n}{2} \log(2\pi) - \frac{1}{2} \log |\Sigma^e| + \sum_{i=1}^n h(z_i) - \frac{1}{2} \mathbb{E}_{\mathbf{e}} \{ \log |\nabla_{\mathbf{e}} f \cdot \nabla_{\mathbf{e}} f^\top| \} \quad (9)$$

where the covariance matrices Σ^e and Σ^a do not depend on the intra-cortical connectivity, because they only depend on \mathbf{x} , \mathbf{y} , and \mathbf{e} :

$$\Sigma^a = \Sigma^{xye} = \begin{pmatrix} \Sigma^x & c_{xy} \cdot \Sigma^x \cdot K^\top & c_{ye} \cdot c_{xy} \cdot \Sigma^x \cdot (F \cdot K)^\top \\ c_{xy} \cdot K \cdot \Sigma^x & \Sigma^y & c_{ye} \cdot \Sigma^y \cdot F^\top \\ c_{ye} \cdot c_{xy} \cdot F \cdot K \cdot \Sigma^x & c_{ye} \cdot F \cdot \Sigma^y & \Sigma^e \end{pmatrix}$$

but, according to [33], $\nabla_{\mathbf{e}} f$ does depend on the intra-cortical connectivity due to the interactions in the Divisive Normalization, c_{ez} and H :

$$\nabla_{\mathbf{e}} f = \mathbb{D}_{\text{sign}(\mathbf{e})} \cdot \mathbb{D}_{(b+c_{ez} \cdot H \cdot |\mathbf{e}|)}^{-1} \cdot [\mathbb{I} - c_{ez} \cdot \mathbb{D}_{\mathbf{z}} \cdot H] \cdot \mathbb{D}_{(\gamma \text{sign}(\mathbf{e})|\mathbf{e}|^{\gamma-1})} \quad (10)$$

where \mathbb{D}_v is a diagonal matrix with the vector v in the diagonal.

Eqs. 9 and 10 explicitly show that $T(\mathbf{x}, \mathbf{y}, \mathbf{z})$ *does* depend on the intra-cortical connectivity.

Another way to see the dependence with the intra-cortical connectivity consist of identifying these two terms in Eq. 9: the (Gaussian) $T(\mathbf{x}, \mathbf{y}, \mathbf{e})$, using the definition in Eq. 6, and the variation of T under the transform $\mathbf{z} = f(\mathbf{e})$, using the property in Eq. 8. By doing that, it is easy to see that:

$$T(\mathbf{x}, \mathbf{y}, \mathbf{z}) = \left(T(\mathbf{x}, \mathbf{y}, \mathbf{e}) - T(\mathbf{e}) \right) + T(\mathbf{z}) \quad (11)$$

where the term in the parenthesis obviously does not depend on the intra-cortical connectivity (because \mathbf{x} , \mathbf{y} and \mathbf{e} are previous to that interaction), but $T(\mathbf{z})$ *does* depend on the Divisive Normalization.

The Mutual Information measures do not capture the effect of intra-cortical connectivity: This is easy to see using the following property: the mutual information is invariant to non-singular differentiable transforms of the random vectors [57]:

$$I(\mathbf{a}, f(\mathbf{b})) = I(\mathbf{a}, \mathbf{b}) \quad (12)$$

²If \mathbf{x} is a Gaussian variable, its entropy in *nats* is $h(\mathbf{x}) = \frac{1}{2} \log |2\pi e \Sigma^x|$ where Σ^x is the covariance of \mathbf{x} [5].

This property is easy to see by considering that $I(\mathbf{a}, \mathbf{b})$ measures the KL-divergence between the densities $p(\mathbf{a}, \mathbf{b})$ and $p(\mathbf{a})p(\mathbf{b})$ [5]. Taking into account that the Jacobian that appears in the variation of the probability under transforms [58] is compensated (in the integral of the KL-divergence) by the change of the differential volume, one gets the invariance.

As a result, no *pairwise* measure I involving \mathbf{x} , \mathbf{y} , and \mathbf{z} depends on the intra-cortical connectivity:

$$\begin{aligned} I(\mathbf{x}, \mathbf{y}) &= \frac{1}{2} \log |\Sigma^x| + \frac{1}{2} \log |\Sigma^y| - \frac{1}{2} \log |\Sigma^{xy}| \\ I(\mathbf{x}, \mathbf{z}) &= I(\mathbf{x}, f(\mathbf{e})) = I(\mathbf{x}, \mathbf{e}) = \frac{1}{2} \log |\Sigma^x| + \frac{1}{2} \log |\Sigma^e| - \frac{1}{2} \log |\Sigma^{xe}| \\ I(\mathbf{y}, \mathbf{z}) &= I(\mathbf{y}, f(\mathbf{e})) = I(\mathbf{y}, \mathbf{e}) = \frac{1}{2} \log |\Sigma^y| + \frac{1}{2} \log |\Sigma^e| - \frac{1}{2} \log |\Sigma^{ye}| \end{aligned} \quad (13)$$

where,

$$\begin{aligned} \Sigma^{xy} &= \begin{pmatrix} \Sigma^x & c_{xy} \cdot \Sigma^x \cdot K^\top \\ c_{xy} \cdot K \cdot \Sigma^x & \Sigma^y \end{pmatrix} \\ \Sigma^{xe} &= \begin{pmatrix} \Sigma^x & c_{ye} \cdot c_{xy} \cdot \Sigma^x \cdot (F \cdot K)^\top \\ c_{ye} \cdot c_{xy} \cdot F \cdot K \cdot \Sigma^x & \Sigma^e \end{pmatrix} \\ \Sigma^{ye} &= \begin{pmatrix} \Sigma^y & c_{ye} \cdot \Sigma^y \cdot F^\top \\ c_{ye} \cdot F \cdot \Sigma^y & \Sigma^e \end{pmatrix} \end{aligned}$$

Therefore, we have demonstrated an important concept: in the biologically plausible *Model I*, Eq. 13 means that the conventional I measures *do not capture* the intra-cortical connectivity, which is critical to get that high correlation with biology. On the contrary, Eqs. 9 and 10 explicitly show that T *does* depend on the intra-cortical connectivity.

3.2 T and I as descriptors of feedback (*Model II*)

In *Model II* there is no nonlinearity so, if the source \mathbf{s} is Gaussian and so are the noises injected at the different layers, all the variables (in the forward pass) will be Gaussian including \mathbf{z} . Then, the considered feedback from \mathbf{z} to \mathbf{x} just injects an extra Gaussian variable back into \mathbf{x} . As a result, \mathbf{x} will be Gaussian too for any strength of the feedback. For slow-varying inputs (as natural images at the retina) the feedback signal (coming from the past) is not totally independent of the current value of the source, so the covariance at the retina is not the sum of the covariance matrices of the separate terms in the sum in the first equation of *Model II*. However, this does not modify the Gaussian assumption.

All these considerations imply that the definitions in terms of entropy given in Eqs. 6 and 7 can be applied together with the expression of the entropy for Gaussian signals that only depends on the corresponding covariance matrices. As a result, in order to make explicit the dependence on feedforward and feedback connectivity one only has to consider all possible covariance matrices, which is what we list below for *Model II*.

Assuming that signal and noise are not correlated, the covariance matrices of the signal at each isolated layer are:

$$\begin{aligned} \Sigma^x &= \mathbb{E}\{x \cdot x^\top\} = \Sigma^s + \Sigma^{n_x} + \left(\frac{c_{zx}}{c_{xy}c_{ye}c_{ez}} \right)^2 F^{-1} \cdot \Sigma^z \cdot F^{-1\top} + \frac{c_{zx}}{c_{xy}c_{ye}c_{ez}} M(s, z) \\ \Sigma^y &= c_{xy}^2 \cdot K \cdot \Sigma^x \cdot K^\top + \sigma^2(n_y) \mathbb{I} \\ \Sigma^e &= c_{ye}^2 \cdot F \cdot \Sigma^y \cdot F^\top + \sigma^2(n_e) \mathbb{I} \\ \Sigma^z &= c_{ez}^2 \cdot \Sigma^e + n_e^2 \cdot \mathbb{I}_d \end{aligned} \quad (14)$$

where $M(s, z)$ is a symmetric matrix that describes the relation between \mathbf{s} and \mathbf{z} (they are not independent), and it is given by: $M(s, z) = F^{-1} \cdot \mathbb{E}\{s \cdot z^\top\} + (F^{-1} \cdot \mathbb{E}\{s \cdot z^\top\})^\top$.

Additionally, the covariance matrices of *two* concatenated vectors that have not been given in Section 3.1 are:

$$\begin{aligned} \Sigma^{xz} &= \begin{pmatrix} \Sigma^x & c_{ye} \cdot c_{xy} \cdot c_{ez} \cdot \Sigma^x \cdot (F \cdot K)^\top \\ c_{ye} \cdot c_{xy} \cdot c_{ez} \cdot F \cdot K \cdot \Sigma^x & \Sigma^z \end{pmatrix} \\ \Sigma^{yz} &= \begin{pmatrix} \Sigma^y & c_{ye} \cdot c_{ez} \cdot \Sigma^y \cdot F^\top \\ c_{ye} \cdot c_{ez} \cdot F \cdot \Sigma^y & \Sigma^z \end{pmatrix} \\ \Sigma^{ez} &= \begin{pmatrix} \Sigma^e & c_{ez} \cdot \Sigma^e \\ c_{ez} \cdot \Sigma^e & \Sigma^z \end{pmatrix} \end{aligned} \quad (15)$$

Similarly, the covariance matrices of *three* and *four* concatenated vectors that have not been given in Section 3.1 are:

$$\begin{aligned} \Sigma^{xyz} &= \begin{pmatrix} \Sigma^x & c_{xy} \cdot \Sigma^x \cdot K^\top & c_{ye} \cdot c_{xy} \cdot c_{ez} \cdot \Sigma^x \cdot (F \cdot K)^\top \\ c_{xy} \cdot K \cdot \Sigma^x & \Sigma^y & c_{ye} \cdot c_{ez} \cdot \Sigma^y \cdot F^\top \\ c_{ye} \cdot c_{xy} \cdot c_{ez} \cdot F \cdot K \cdot \Sigma^x & c_{ye} \cdot c_{ez} \cdot F \cdot \Sigma^y & \Sigma^z \end{pmatrix} \\ \Sigma^{xez} &= \begin{pmatrix} \Sigma^x & c_{xy} \cdot c_{ye} \cdot \Sigma^x \cdot (F \cdot K)^\top & c_{ye} \cdot c_{xy} \cdot c_{ez} \cdot \Sigma^x \cdot (F \cdot K)^\top \\ c_{xy} \cdot c_{ye} \cdot F \cdot K \cdot \Sigma^x & \Sigma^e & c_{ez} \cdot \Sigma^e \\ c_{ye} \cdot c_{xy} \cdot c_{ez} \cdot F \cdot K \cdot \Sigma^x & c_{ez} \cdot \Sigma^e & \Sigma^z \end{pmatrix} \quad (16) \\ \Sigma^{xyez} &= \begin{pmatrix} \Sigma^x & c_{xy} \cdot \Sigma^x \cdot K^\top & c_{ye} \cdot c_{xy} \cdot \Sigma^x \cdot (F \cdot K)^\top & c_{ye} \cdot c_{xy} \cdot c_{ez} \cdot \Sigma^x \cdot (F \cdot K)^\top \\ c_{xy} \cdot K \cdot \Sigma^x & \Sigma^y & c_{ye} \cdot \Sigma^y \cdot F^\top & c_{ye} \cdot c_{ez} \cdot \Sigma^y \cdot F^\top \\ c_{ye} \cdot c_{xy} \cdot F \cdot K \cdot \Sigma^x & c_{ye} \cdot F \cdot \Sigma^y & \Sigma^e & c_{ez} \cdot \Sigma^e \\ c_{ye} \cdot c_{xy} \cdot c_{ez} \cdot F \cdot K \cdot \Sigma^x & c_{ye} \cdot c_{ez} \cdot F \cdot \Sigma^y & c_{ez} \cdot \Sigma^e & \Sigma^z \end{pmatrix} \end{aligned}$$

Given the matrices in Eqs. 14-16, in *Model II* both variables T and I depend on the intra-cortical connectivity c_{ez} and on the feedback c_{zx} . However, the sensitivity of the descriptors is not that obvious from these equations plugged into Eqs. 6 and 7. Therefore, in order to figure out which descriptor is better (which one is more sensitive) one should consider specific values of the parameters (as for instance what we considered in Section 2), and compute T and I in a range of connectivity values.

We do that in the next experimental section where we find that, in *Model II*, our descriptor, T , is substantially more sensitive than I to the feedback, c_{zx} , and the intra-cortical connectivity, c_{ez} . And this happens both for Gaussian signals and also for natural images.

4 Empirical results

In this experimental section³ we address the following points:

- We use the theoretical expressions to illustrate the behaviors of T and I , both in the case where the superiority of T is analytically obvious (as in Eqs. 9-11 versus Eqs. 13 for the intra-cortical connectivity in *Model I*), and in the case where the behavior is not easy to see directly from Eqs. 14-16 plugged into Eqs. 6-7 (in *Model II*). In these experiments we use Gaussian sources with the same mean and covariance as natural images and the model parameters discussed in Section 2.4.
- We confirm the theoretical results presented in Section 3 for both models (I and II) through a specific empirical estimator of T and I [12, 59] that has been already used in visual neuroscience [10, 11]. This empirical confirmation of the theory uses sets of $0.5 \cdot 10^5$ Gaussian samples injected into the models (I and II), and then, the empirical estimator is applied to the responses of the models. Incidentally, the presented pair *theory-data* is a good test-bed for empirical estimators of T and I .
- We explore how the empirical estimations of T and I behave for natural (non-Gaussian) images where, in principle, the theory would not be applicable. We also use sets of $0.5 \cdot 10^5$ natural image patches and the same variations of *Model I* and *Model II*.
- We explore the behavior of T and I in real fMRI signals from cortical regions V1, V2, V3, V4 responding to natural images so that we can discuss possible connectivity schemes.

The structure of this section is as follows: (1) We describe the experimental methods: the empirical estimator, the natural and synthetic image data, and computational issues of the theoretical expressions. (2) We present T and I surfaces for different intra-cortical connectivity c_{ez} and α_H that controls H in *Model I*. (3) We present T and I surfaces for different feedforward and feedback connectivity c_{ez} and c_{zx} in *Model II*. Finally, (4) we present the empirical estimations of T and I from real fMRI recordings.

4.1 Methods: empirical estimator, data, and computational issues

Empirical estimation of T and I from samples: here we use the *Rotation-Based Iterative Gaussianization* (RBIG). This method, originally proposed for PDF estimation [12], is able to transform data following any multivariate PDF

³Code and data at http://isp.uv.es/docs/CODE_connectivity.zip, [Samples.tar.gz](http://isp.uv.es/docs/Samples.tar.gz), and [DATA_connect_2.zip](http://isp.uv.es/docs/DATA_connect_2.zip)

into data that follows a unit-covariance multivariate Gaussian. In this way, RBIG is useful to estimate the redundancy among coefficients because it accumulates the variations in redundancy while transforming the original dataset into the final Gaussian dataset where all coefficients are independent. The advantages of RBIG with regard to other information estimators [16, 17] has been shown in [11, 59, 60]. RBIG has also been used in visual neuroscience to check the *Efficient Coding Hypothesis* in Wilson-Cowan networks [10], in Divisive Normalization networks [11], and in color appearance networks [61]. However, any other empirical estimator of T and I from samples [13–17] could be used in the experiments below.

Natural and synthetic data: In the experiments we used $0.5 \cdot 10^5$ image patches of size 8×8 , i.e. $n = 64$, randomly taken from the luminance component of two colorimetrically-calibrated datasets: the IPL dataset [62, 63], and the Barcelona dataset [64]. In the IPL dataset only images under the CIE D65 (daylight-like) illuminant were considered. The two datasets were linearly scaled so that the average luminance in both was equal to 40 cd/m^2 . This separate global normalization ensures that image patches from both sets are equivalent and can be safely mixed. Then, we randomly extracted the samples $0.25 \cdot 10^5$ from each dataset, and we computed the covariance from this joint set of $0.5 \cdot 10^5$ samples: see Σ^s in Fig. 4. This matrix, Σ^s , is the starting point of all the theoretical results presented in Section 3. Our data has the classical covariance of the luminance in natural images (see for instance [65]), which is diagonalized by DCT-like basis functions (see Fig. 4, consistently with [25, 63, 66]). Then, we generated $0.5 \cdot 10^5$ Gaussian vectors of dimension $n = 64$ with the mean and covariance of the natural samples. Of course, both sets (natural and synthetic) are not the same (as can be seen in Fig. 4, consistently with [18, 19]). Then, we inject the synthetic and natural samples through *Model I* and *Model II* to get the corresponding responses x , y , e , and z , for the range of connectivity values considered in Section 2.

Computational issues: All the analytical results (e.g. Eq. 9) depend on the computation of determinants of large matrices (either covariance matrices or the Jacobian $\nabla_{ef}^T \cdot \nabla_{ef}$). The computation of determinants in high-dimensional scenarios is very prone to divergences to 0 or ∞ . Therefore, it is better to avoid its computation: given the fact that the

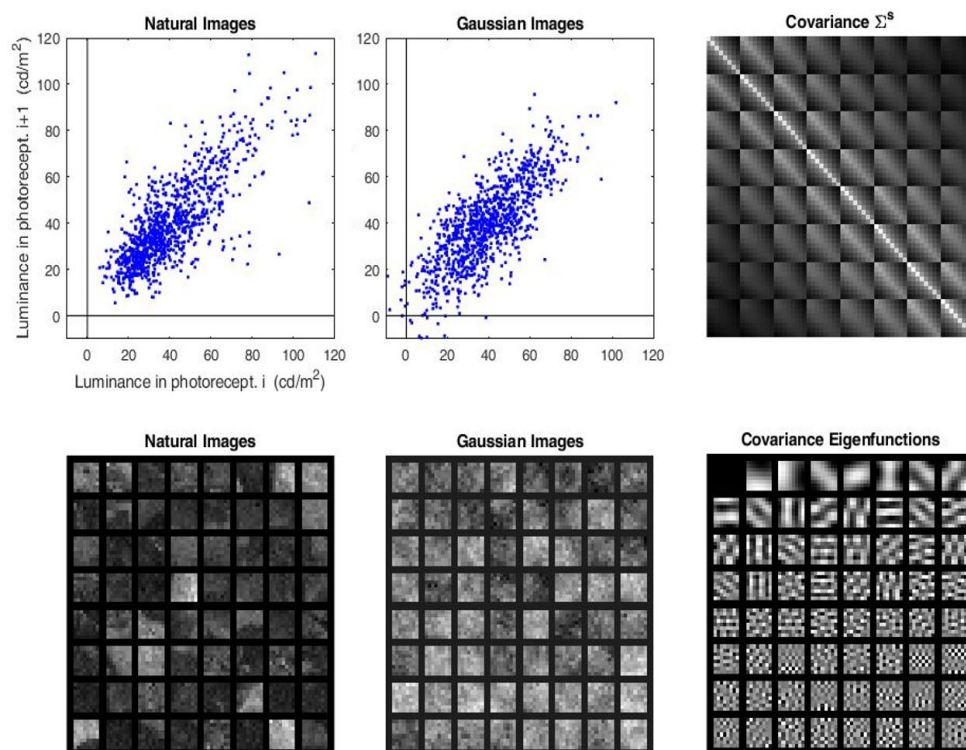


Figure 4: Natural and synthetic image data (the source s). The bottom-left mosaic shows illustrative samples from the colorimetrically-calibrated databases IPL and Barcelona. The top-left scatter plot illustrates the joint PDF of the luminance at neighbor photoreceptors. Images and scatter plot show the (non-Gaussian) bias towards low-luminance, and the spatial smoothness of the signal (predominance of low spatial frequency). The non-diagonal nature of the covariance matrix (at the top-right) captures the spatial smoothness, and its eigenfunctions (bottom-right) are similar to the frequency analyzers in the cortex models (in Fig. 1). The order of the functions according the eigenvalue confirms the low-frequency nature of the signal. The central column shows Gaussian samples with the same mean and covariance.

considered matrices, A , are symmetric (either Σ or $\nabla_e f^\top \cdot \nabla_e f$), they are diagonalizable by an orthonormal transform (with unit determinant). Therefore, it holds $\log|A| = \sum_{i=1}^d \log(\lambda_i)$ where λ_i are the eigenvalues of A (whatever the dimension $d \times d$ of the matrix A). Note that this sum is more robust than the naive computation of the determinant.

4.2 Results for I and T in terms of nonlinear intra-cortical connectivity (*Model I*)

Figure 5 shows the results of Mutual Information for different intra-cortical connectivity scenarios in the nonlinear *Model I*. Specifically, we show (a) the theoretical results for Gaussian signals, (b) the empirical results computed with RBIG for Gaussian signals, and (c) the empirical results computed with RBIG for natural signals.

We see two basic trends in the results (both in the theory and in the empirical estimations):

1. $I(x, y) \approx I(x, z) \ll I(y, z)$. This could be expected because the shared information is reduced with the noise introduced in each layer and $\sigma(\mathbf{n}_y) \gg \sigma(\mathbf{n}_e)$, and no noise is introduced in z , i.e. $f(\cdot)$ is invertible. Therefore, more information is lost between x and inner layers (either y or z), than the information lost between y and z , which have an almost invertible relation: only a small fraction of bits is lost due to \mathbf{n}_e .
2. More important for the description of connectivity is the fact that (as predicted by the theory), Mutual Information is *totally insensitive* to the differences in intra-cortical connectivity. Therefore, this pairwise measure is not a good descriptor of connectivity for this kind of nonlinearity.

It is important to note that these global trends in the theory are consistently confirmed by the empirical estimations. Beyond a small bias (overestimation) in I_{RBIG} , it identifies the substantially bigger connection between y and z rather than between x and inner layers. Moreover, I_{RBIG} is also constant over the range of nonlinear connectivity values.

Interestingly, the empirical results for natural images also follow these trends even though the signals are no longer Gaussian. In this case, the non-Gaussianity only introduces a reduction in the I_{RBIG} estimates and a small variation over the explored models, which is negligible in terms of describing changes in the connectivity.

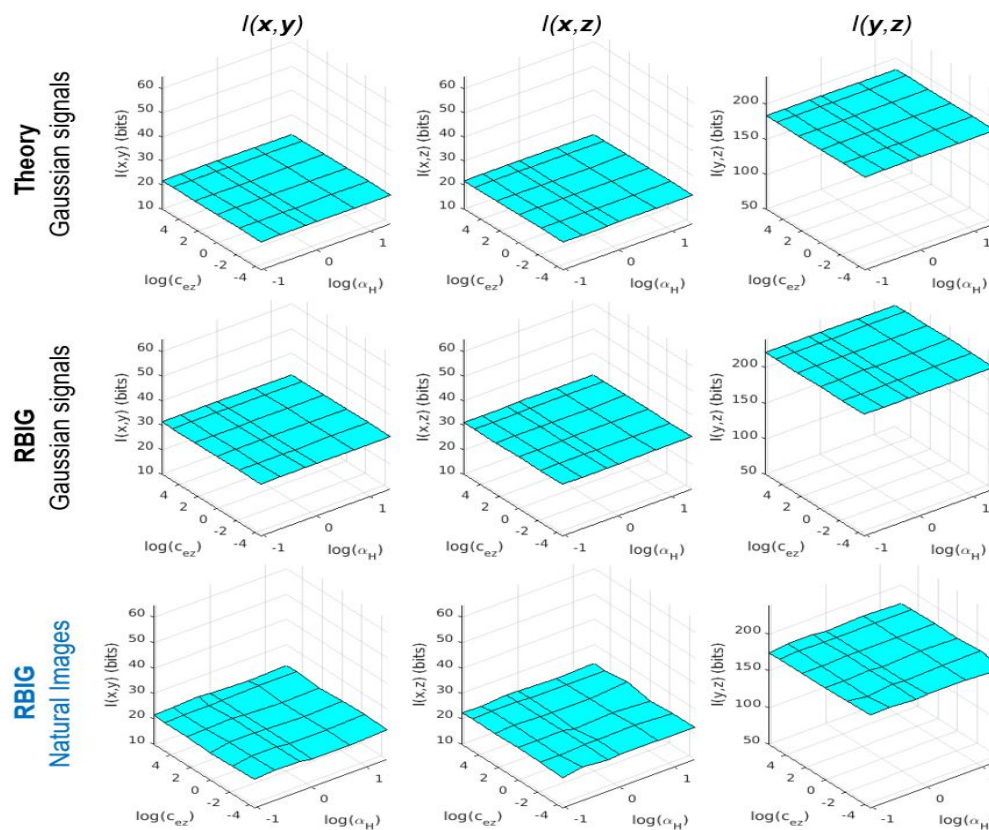


Figure 5: Mutual Information does not describe intra-cortical connectivity in *Model I*. Plots of I as a function of intra-cortical connectivity for Gaussian signals (theory and RBIG estimates), and empirical results for natural images.

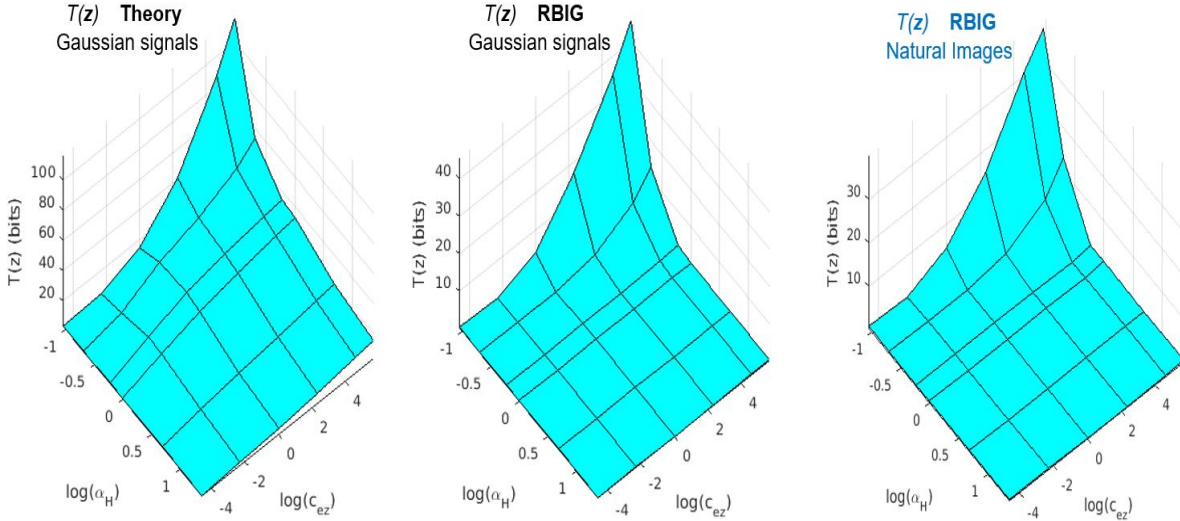


Figure 6: Total Correlation does capture variations in intra-cortical connectivity in *Model I*. Plots of $T(z)$ as a function of intra-cortical connectivity for Gaussian signals (theory and RBIG estimates), and empirical results for natural images.

Figure 6 shows the part of $T(x, y, z)$ that depends on the nonlinear connectivity: $T(z)$ according to Eq. 11. In this case, as opposed to I , the *Total correlation* strongly depends on the intra-cortical connectivity.

Again, (beyond a subestimation bias in RBIG) the general trend of the empirical estimations over the connectivity range confirms the theoretical predictions. The non-Gaussianity of natural signals does not introduce major deviations in the trend of the surface.

A technical comment on the estimation of $T(z)$: as the variables $z = f(e)$ are non-Gaussian, and this non-Gaussianity is particularly strong in some regions of the explored domain of connectivity, it is important to use a large number of iterations in the Gaussianization algorithm to get a good estimate of T . In particular here we used 500 iterations.

4.3 Results for I and T in terms of feedforward and feedback connectivity (*Model II*)

Figure 7 shows the results of Mutual Information for different feedforward and feedback connectivity scenarios: different combinations of c_{ez} and c_{zx} in *Model II*. Specifically, we show: (a) the theoretical results for Gaussian signals, (b) the empirical results computed with RBIG for Gaussian signals, and (c) the empirical results computed with RBIG for natural signals.

As in the recurrent *Model II* the interpretation of the analytical results is more complicated, in this section each surface is given in a relative scale with regard to its maximum so that the sensitivity of the different descriptors can be fairly compared. Moreover, the variation of the descriptor, Δ , both in percentage and in bits, is also given. As the explored range is the same for every descriptor, Δ is a good measure of the sensitivity to the considered variation of the connectivity.

In *Model II*, due to the top-down feedback signal, $x \xleftarrow{c_{zx}} z$, in principle, all the layers can be affected by an enhanced transmission at a deep layer such as, $e \xrightarrow{c_{ez}} x$. Specifically, the results show the following trends:

1. In general, the shared information increases with c_{ez} . This is obvious in the cases where z is one of the considered nodes (e.g. the last three columns $I(x, z)$, $I(y, z)$ or $I(e, z)$) because an increased c_{ez} improves the presence of the source in the inner representation. More interestingly, we can see that when z is not considered, the effect of c_{ez} is only relevant when there is also significant feedback (as in the two first columns $I(x, y)$ and $I(x, e)$). This is also the case when considering nodes that are far away, as in $I(x, z)$.
2. When considering nodes that are far from the considered interactions (e.g. y and e) the descriptor is insensitive to the variations of connectivity (see $I(y, e)$ in the third column).
3. In summary, the average percentage of variation of the measures based on I in the theoretical expressions is $\Delta_I = 47 \pm 30$ %.

For *Model II* the global trends in the theory are consistently confirmed by the empirical estimations. Similarly to what we found in *Model I*, parallel results in the theory and empirical estimates also form *Model II* confirm the correctness of the theory and the appropriateness of RBIG in this application.

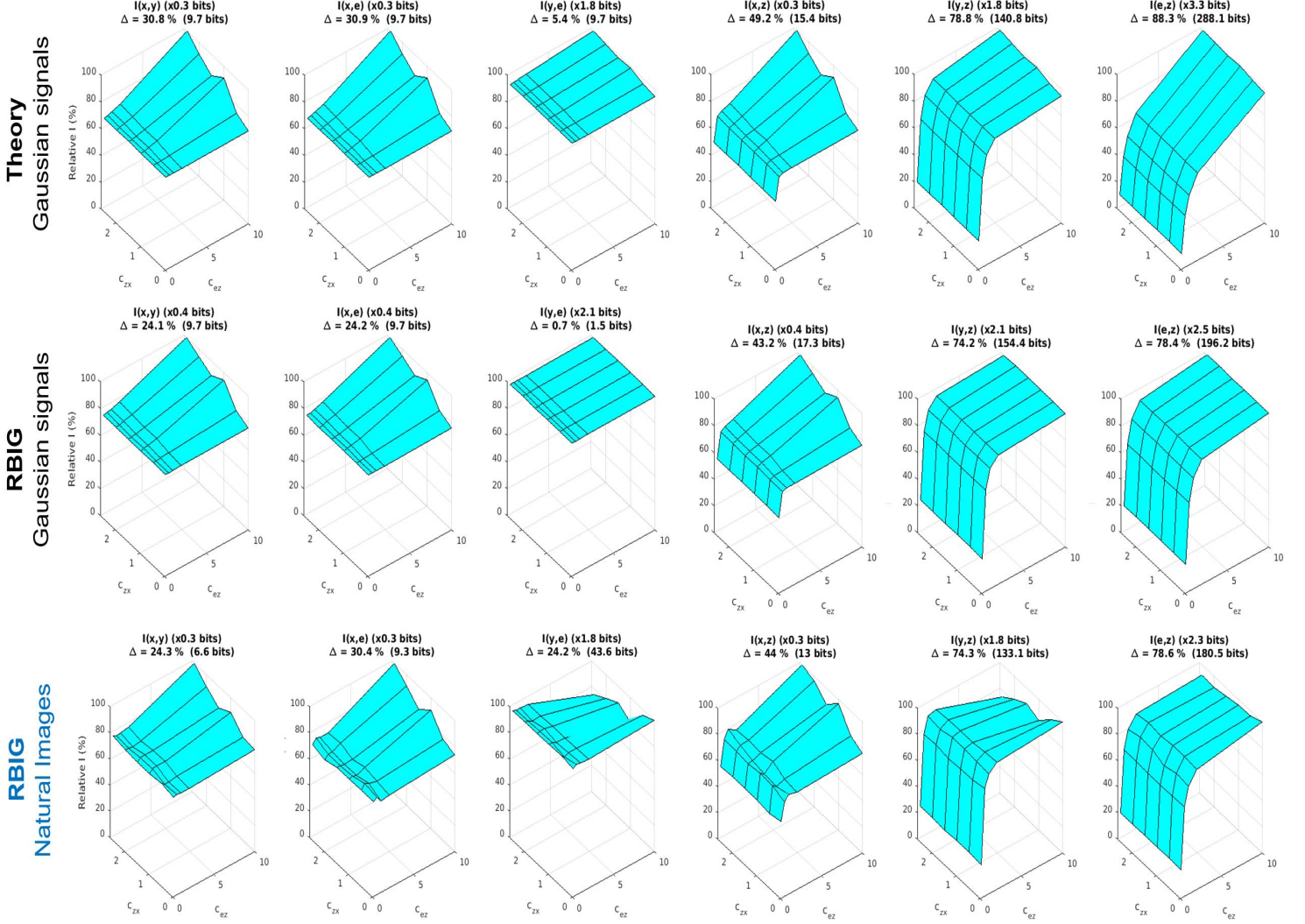


Figure 7: Mutual Information has mild dependence with feedforward and feedback connectivity in *Model II*. Plots of I as a function of the feedforward connectivity, c_{ez} , and feedback, c_{zx} , for Gaussian signals (theory and RBIG estimates), and empirical results for natural images. The plots display relative values of I in percentage with regard to the maximum together with a factor (e.g. $\times 0.3$ in the top-left plot) that allows to express this percentage in absolute values (in bits). Moreover, the plots display the variation (in bits) of the considered descriptor over the range of connectivity values (e.g. $\Delta = 9.7$ bits in the top-left plot). This is a measure of the sensitivity of the descriptor.

Moreover, the empirical results for natural images also follow these trends even though the signals are no longer Gaussian. In this case, the non-Gaussianity only introduces a noticeable variation in $I(y, e)$. However, this does not change much the global sensitivity of I , as described by Δ .

Figure 8 shows the results of Total Correlation for different feedforward and feedback connectivity scenarios: different combinations of c_{ez} and c_{zx} in *Model II*. As above, we show: (a) the theoretical results for Gaussian signals, (b) the empirical results computed with RBIG for Gaussian signals, and (c) the empirical results computed with RBIG for natural signals. Here we also present the T surfaces in relative scale for a simpler comparison with the I surfaces in Fig. 7.

The overall percentage of variation of the measures based on T in the theoretical expressions is $\Delta_T = 75 \pm 11 \%$.

In the recurrent *Model II*, the sensitivity of T to connectivity and feedback is stronger than the sensitivity of I . Note that $\Delta_T > \Delta_I$ with substantially lower variance over the considered nodes. Therefore, T is more appropriate than I to describe the connectivity in the recurrent *Model II*.

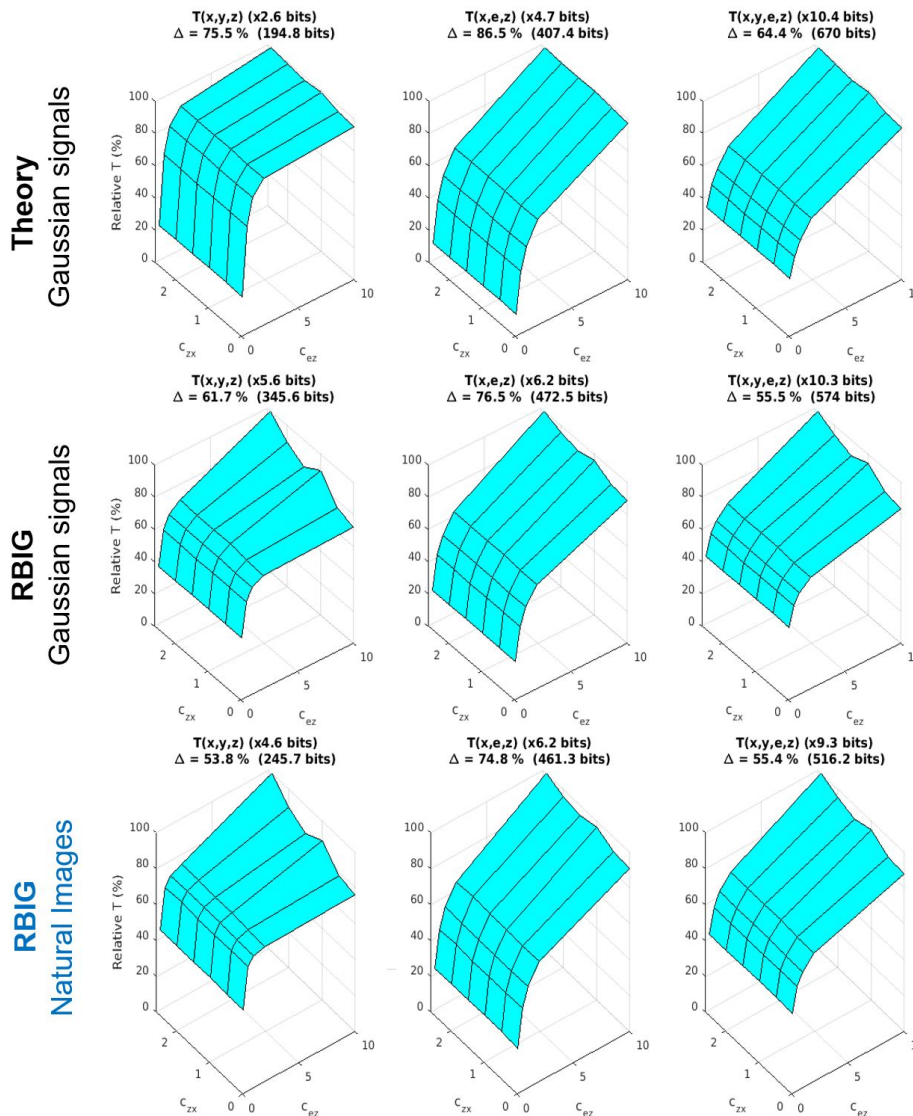


Figure 8: Total Correlation strongly depends on the feedforward and feedback connectivity in *Model II*. Plots of T as a function of the feedforward connectivity, c_{ez} , and feedback, c_{zx} , for Gaussian signals (theory and RBIG estimates), and empirical results for natural images. The plots display relative values of T in percentage with regard to the maximum together with a factor (e.g. $\times 2.6$ in the top-left plot) that allows to express this percentage in absolute values (in bits). Moreover, the plots display the variation (in bits) of the considered descriptor over the range of connectivity values (e.g. $\Delta = 195$ bits in the top-left plot). This is a measure of the sensitivity of the descriptor.

Moreover, as in the previous examples, the empirical estimates from the samples confirm the general trends of the theory, and the results for natural signals approximately follow the results for Gaussian sources.

4.4 Results with real fMRI signals from visual regions V1, V2, V3 and V4

Here we measure the information shared by different visual regions the visual cortex starting from V1. This represents an interesting application because (1) there is a debate on how these regions actually interact [67–71], and (2) there is a long-standing concept in visual neuroscience that relates neural connectivity with information transmission: the *Efficient Coding Hypothesis*, where redundancy reduction has a central role [72, 73]. Specifically, here we take neural data from the *Algonauts Project 2021 challenge* [22], and we consider fMRI signals from V1, V2, V3 and V4 while the observers were looking at natural videos. In our experiments we consider pairwise and multivariate relations among

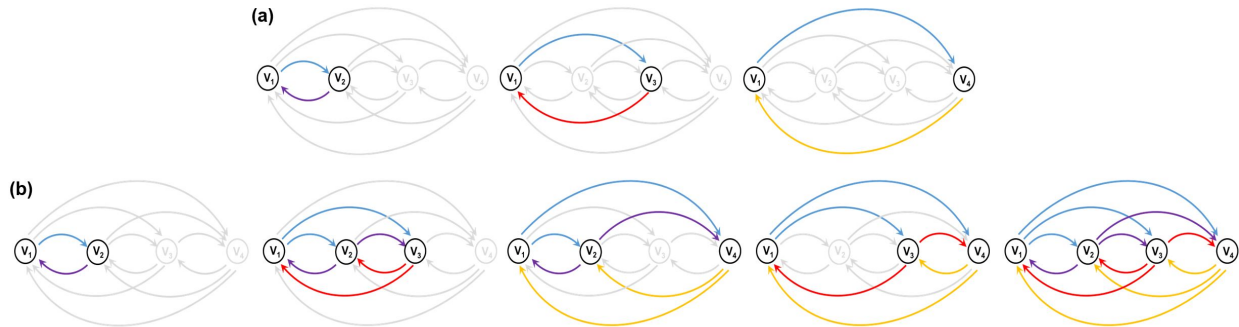


Figure 9: Examples of the (a) pairs of nodes, and (b) groups of nodes, that we consider in our measurements. The top row (a) considers the relation between certain node (in this case V_1), and, from left to right, nodes progressively distant: V_2, V_3 , and V_4 . The bottom row (b), from left to right, adds nodes to the group under consideration. If we start from V_i , the added nodes can be close to it, e.g. (V_i, V_{i+1}, V_{i+2}) in the 2nd diagram, or they can be progressively farther away, as (V_i, V_{i+1}, V_{i+3}) or (V_i, V_{i+2}, V_{i+3}) , as in the 3rd and 4th diagrams. Finally, the last diagram at the right shows that we can consider all nodes at the same time, namely (V_1, V_2, V_3, V_4) .

regions which (anatomically) are progressively farther away. However, our descriptors of functional links do not make any prior assumption of the possible feedforward or feedback connections.

Ensembles: The considered dataset provides 3 responses of 9 observers for 1000 natural videos in a number of voxels of the considered regions (V_1, V_2, V_3 and V_4). In this database there is a one-to-one relation between input and responses, but the number of available voxels depends on the observer and the cortical region. Therefore, just for illustrative purposes, we take 20 randomly selected voxels per region for each observer. This means 20-dimensional signals associated to one input. By considering the data of all trials, all observers, and all input videos, we have $3 \times 9 \times 1000 = 27000$ samples of these 20-dimensional vectors for each region. In these ensembles, the i -th vector of each region corresponds to the same input and the same observer, but the j -th dimension of the vector is the response of a randomly chosen voxel in that region (and observer). We assume all the observers and all the voxels in a region are equivalent. By rerunning this random selection of voxels we get equivalent ensembles.

Empirical estimation: Given the fact that the marginal PDFs of the signals are approximately Gaussian (results not shown), in the estimations of T and I based on iterative Gaussianization we chose only 20 iterations (as opposed to the 500 iterations used in *Model I* where z is non-Gaussian). We re-estimate T and I from equivalent, randomly chosen, ensembles 30 times and we report the average and standard deviation of the results.

Measurements of functional links: we measured I and T in all possible distinct combinations of nodes. Figure 9 illustrates pairwise and multivariate relations among regions which (anatomically) are progressively farther away. Note that the functional link of the configurations in the top row can be addressed by the pairwise $I(\mathbf{v}_i, \mathbf{v}_j)$ or $T(\mathbf{v}_i, \mathbf{v}_j)$. However, progressive consideration of additional nodes, as in the bottom row, can only be quantified using a multivariate descriptor $T(\mathbf{v}_i, \mathbf{v}_j, \mathbf{v}_k, \dots)$. Note that in a case where the connections are unknown, the shared information (either I or T) is not only affected by the *direct* connections between the considered nodes (in our figure *direct* connections are in color), but also by all other possible *indirect* connections (depicted in gray). The *indirect* connections imply communication through alternative regions that may re-inject the relevant signal into the considered nodes and have a positive effect in the functional link.

On top of the two-node and multi-node cases, mono-mode references are convenient to know if the information is lost through the network or, on the contrary, there are positive synergies. To this end, we report three additional numbers: $T(\mathbf{v}_i)$, which is a measure of the redundancy within the node \mathbf{v}_i ; and also $I(\mathbf{v}_i, \mathbf{v}_i)$, and $T(\mathbf{v}_i, \mathbf{v}_i)$. In principle, the information shared by a variable with itself, as in $I(\mathbf{v}_i, \mathbf{v}_i)$, and $T(\mathbf{v}_i, \mathbf{v}_i)$, is ∞ ⁴. However, given the uncertainty we introduce when using random voxels from each region/observer, two (randomly chosen) sets of \mathbf{v}_i are not aligned and then $I(\mathbf{v}_i, \mathbf{v}_i)$, and $T(\mathbf{v}_i, \mathbf{v}_i)$ do not diverge to ∞ . Instead, they are measures of the common information present in every realization of the ensemble of responses of that node \mathbf{v}_i . Therefore, they are a convenient reference to know if the consideration of extra nodes increases or decreases this mono-mode amount of information.

⁴Given any n -dimensional variable \mathbf{a} , the samples of (\mathbf{a}, \mathbf{a}) are aligned in a $2n$ -dimensional space, and then the joint differential entropy terms of Eqs. 6-7 is $-\infty$, leading to $I(\mathbf{a}, \mathbf{a}) = T(\mathbf{a}, \mathbf{a}) = \infty$.

For a more intuitive comparison of the results corresponding to configurations with different number of nodes, we report the shared information *per node*. This means: $I(\mathbf{v}_i, \mathbf{v}_j)/2$, $T(\mathbf{v}_i, \mathbf{v}_j)/2$, $T(\mathbf{v}_i, \mathbf{v}_j, \mathbf{v}_k)/3$, and, $T(\mathbf{v}_1, \mathbf{v}_2, \mathbf{v}_3, \mathbf{v}_4)/4$. In the case of $T(\mathbf{v}_i)$ the definition already has a single node, so *bits* and *bits/node* are the same.

Finally, we report not only the absolute values in *bits/node*, but (more interestingly to describe the connectivity) how the information per node increases or decreases when we go way from one node or include progressively distant nodes in the measure. We give this deviation in % with regard to the information per node in V1 (either $I(\mathbf{v}_1, \mathbf{v}_1)$ or $T(\mathbf{v}_1, \mathbf{v}_1)$).

Results: Tables 1-2 show the measures of shared information in three panels: the top panel shows the pair-wise measures $I(\mathbf{v}_i, \mathbf{v}_j)$, the middle panel shows the single-node measure $T(\mathbf{v}_i)$, and the bottom panel shows the multi-node measures $T(\mathbf{v}_i, \mathbf{v}_j, \dots)$. Table 1 has absolute measures in *bits/node*, and Table 2 displays the variation (in %) of the considered configuration with regard to the corresponding measure in V1. The $T(\mathbf{v}_i, \mathbf{v}_j, \dots)$ panels have a pair-wise part (at the left) and a multi-node part (the last four columns). This multi-node parts have to be read *row-wise*: each number reports how the node in the row interacts with the nodes in the different columns. Moreover, the consideration of extra nodes is done in cyclic way: in the 3rd row $v_i = v_3$, and hence the 5th column, $(v_{i+1}, v_{i+2}) = (v_4, v_1)$, refers to the connectivity among the nodes (v_3, v_4, v_1) .

Not all the values in the tables are independent because of the symmetry of the measures. Note that I and T are invariant to the permutation of the variables: $I(\mathbf{v}_i, \mathbf{v}_j) = I(\mathbf{v}_j, \mathbf{v}_i)$, and $T(\mathbf{v}_i, \mathbf{v}_j, \mathbf{v}_k) = T(\mathbf{v}_j, \mathbf{v}_k, \mathbf{v}_i) = \dots$. This implies that the I panels are symmetric and so it is the pairwise part of the T panels. Also as a consequence of the invariance to permutation, some multi-node configurations are equivalent. As the order does not matter, we have combinations of 4 nodes taken 3 at a time, i.e. only 4 independent node configurations. For the sake of clarity the non-redundant values of the tables are highlighted in blue. Also for clarity, the standard deviation over the 30 realizations of the estimation has been reported only in the independent values of Table 1.

The discussion of the results will be focused on the variations of information as we depart from a node (Table 2). Departure, as in the top row of Fig. 9, means *moving away from the diagonal* (along rows/columns) in the pairwise parts of the tables. Departure, as in the bottom row of Fig. 9, means *moving to the right* (for the highlighted numbers) in the multi-node parts. Table 1, with the original absolute measures, is just given for completeness and for the reader convenience.

A final comment on the absolute magnitudes: in every case, the estimated $T(\mathbf{v}_i, \mathbf{v}_j) > I(\mathbf{v}_i, \mathbf{v}_j)$, which is consistent with the definitions because (as discussed in Eqs. 6-7) T includes the redundancy within the nodes and hence the information is necessarily bigger.

Information flow and conjectures on connectivity: Results show that the redundancy within each node $T(\mathbf{v}_i)$ is smaller in deeper layers than in V1 (see the negative increments in the middle panel of Table 2). This is consistent with the *Efficient Coding Hypothesis* [72, 73].

$I(\mathbf{v}_i, \mathbf{v}_j)$ (in bits/node)	v_1	v_2	v_3	v_4
v_1	2.4 ± 0.3	1.3 ± 0.2	1.0 ± 0.2	0.8 ± 0.1
v_2	1.3	2.0 ± 0.2	1.2 ± 0.2	0.7 ± 0.1
v_3	1.0	1.2	1.7 ± 0.3	0.8 ± 0.1
v_4	0.8	0.7	0.8	2.2 ± 0.3

$T(\mathbf{v}_i)$ (in bits/node)	v_1	v_2	v_3	v_4
	3.6 ± 0.3	3.2 ± 0.2	3.0 ± 0.2	3.5 ± 0.3

$T(\mathbf{v}_i, \mathbf{v}_j, \dots)$ (in bits/node)	v_1	v_2	v_3	v_4	v_{i+1}, v_{i+2}	v_{i+1}, v_{i+3}	v_{i+2}, v_{i+3}	$v_{i+1}, v_{i+2}, v_{i+3}$
v_1	6.0 ± 0.3	5.0 ± 0.2	4.7 ± 0.2	4.6 ± 0.3	6.1 ± 0.2	5.9 ± 0.3	5.7 ± 0.3	6.6 ± 0.2
v_2	5.0	5.4 ± 0.3	4.7 ± 0.3	4.5 ± 0.3	5.7 ± 0.3	6.1	5.9	6.6
v_3	4.7	4.7	5.1 ± 0.2	4.5 ± 0.2	5.7	5.7	6.1	6.6
v_4	4.6	4.5	4.5	5.9 ± 0.3	5.9	5.7	5.7	6.6

Table 1: $I(\mathbf{v}_i, \mathbf{v}_j)$ between pairs of areas, $T(\mathbf{v}_i)$ in each area, and $T(\mathbf{v}_i, \mathbf{v}_j, \dots)$ among multiple areas in *bits/node*. See the **Results** paragraph in the text for the interpretation of pairs and triplets with progressively distant nodes.

Reduction in $T(v_i)$ in the middle panel is not the same as the reductions of $T(v_i, v_i)$ or $I(v_i, v_i)$ along the diagonal of the pairwise parts of the top and the bottom panels. While redundancy reduction in $T(v_i)$ means better information encoding, reduction in $T(v_i, v_i)$ or $I(v_i, v_i)$ means a decay in the information content. This decay is more apparent in $I(v_i, v_i)$, because the reduction of $T(v_i, v_i)$ is biased by the simultaneous reduction of the intra-node redundancy in $T(v_i)$. Actually, if we discount $\Delta T(v_i)$ from $\Delta T(v_i, v_i)$, the corrected $T(v_i, v_i)$ is more constant⁵. This smaller reduction in the information content may be a positive effect of connectivity seen in T and not in I .

However, the mono-node measures mentioned above only describe the information in each node, but not how much of this information comes from another region. This second concept, more related to connectivity, is measured by pairwise and multi-node measures. In this regard, progressively bigger reductions in the pairwise $\Delta I(v_i, v_j)$ and $\Delta T(v_i, v_j)$ away from the diagonal mean information loss along the way (or reduced functional connectivity). This information loss seems consistent with the *data processing inequality* [5] to a certain extent. However, as discussed below, the results (particularly T in multiple nodes) confirm the existence of relevant feedback in these regions.

The *data processing inequality* [5] states that information lost between two nodes cannot be recovered by further processing (with no additional input from the original node). This inequality strictly holds in purely feedforward schemes $v_1 \rightarrow v_2 \rightarrow v_3 \rightarrow v_4$, where, due to the absence of feedback connections and skip connections, the response in inner layers conditioned to the previous layer is independent of the early layers. In such systems, it holds $I(v_1, v_2) > I(v_1, v_3) > I(v_1, v_4)$. This behavior is what is observed in the rows of the I panel when moving away from the diagonal to inner layers. This suggests that the feedforward component of the connectivity can be strong, and in such simplistic situation, one could deduce the strength of each connection from the different decays in $I(v_i, v_j)$.

However, in our case (where feedback and skip connections may exist) the *data processing inequality* may not hold. Reductions in I do not necessarily mean that the other connections are not present. This is more clear looking at the results of T . While the behavior of the pairwise T moving to deeper layers is negative (similarly to I), something different happens by considering extra nodes. Under the purely feedforward assumption extra nodes should share less information with the previous and the global T should decrease, particularly if the intra-node redundancy does not increase (as in this pathway). However, we see that in some cases the consideration of extra nodes implies an increase of the shared information per node, as for instance when going from (v_1, v_2) to (v_1, v_2, v_3) or from there to (v_1, v_2, v_3, v_4) (see the positive increments highlighted in blue in Table 2).

Multi-node results obtained from the proposed measure T are interesting because we can see that the connections in the group (v_1, v_2, v_3) are substantially stronger than the connections in the group (v_2, v_3, v_4) despite they are at similar anatomical distance. This suggests some top-down feedback from v_3 or v_2 or feedforward skip connections from v_1 to v_3 . The same is true when considering all the nodes together with a substantial increment (by 11%).

These two different synergistic behaviors that can be seen using the proposed *Total Correlation* clearly mean that one can rule out a pure feedforward scheme in the V_1, V_2, V_3, V_4 regions, and more complex connectivity schemes do exist. This is not that obvious just using the conventional I .

5 Discussion and conclusions

Analytical results: T is a better descriptor of connectivity than I . The goal of this paper is addressing the fundamental limitation of the seminal work that proposed T as a measure of functional connectivity [3]: namely the lack of analytical results that can justify the superiority of the T over the conventional I beyond the multivariate versus pairwise definitions. Here we did that analytical study in the context of the early visual brain with simple models of the retina-V1 cortex pathway.

For mathematical convenience we considered two variations of the general framework presented in Eq. 2: *Model I* and *Model II*. These models were chosen to illustrate two fundamental properties of neural architectures in early vision: (1) the Divisive Normalization nonlinearity in *Model I*, in Section 2.1, and (2) an eventual top-down recurrence in *Model II* in Section 2.2.

It is important to stress again that the models are not arbitrary: according to the results in Section 2.4 the nonlinearity in *Model I* is key to improve the explanation of the psychophysics, and the explored range of intra-cortical connectivity actually covers different behaviors (with substantial differences in the explained variance of human data). The top-down connection in *Model II* was not specifically justified, but given the observed behavior of the steady state in e , the explored feedback does not reduce substantially the $\rho = 0.7$ result. This indicates that *Model II* has certain biological plausibility, so that it can be used to illustrate the study of recurrent connections. The plausibility of the models and the

⁵Losses ΔT corrected in this way (-8.3%, -12.5%, and 0%, for v_2, v_3, v_4), are smaller than the original values (-8.8%, -14.5%, -0.1%), seen in the diagonal of the pairwise part of the T panel (Table 2).

$\Delta I(v_i, v_j)$ (in %)	v_1	v_2	v_3	v_4
v_1	0.0	-45.0	-55.6	-67.0
v_2	-45	-16.1	-47.7	-71.4
v_3	-55.6	-47.7	-26.1	-67.8
v_4	-67.0	-71.3	-67.8	-7.1

$\Delta T(v_i)$ (in %)	v_1	v_2	v_3	v_4
	0.0	-11.1	-15.5	-2.1

$\Delta T(v_i, v_j, \dots)$ (in %)	v_1	v_2	v_3	v_4	v_{i+1}, v_{i+2}	v_{i+1}, v_{i+3}	v_{i+2}, v_{i+3}	$v_{i+1}, v_{i+2}, v_{i+3}$
v_1	0.0	-16.0	-21.3	-21.7	2.3	-1.4	-3.8	11.3
v_2	-16.0	-8.8	-21.4	-23.8	-3.9	2.3	-1.4	11.3
v_3	-21.3	-21.4	-14.5	-24.9	-3.8	-3.9	2.3	11.3
v_4	-21.7	-23.8	-24.9	-0.1	-1.4	-3.8	-3.9	11.3

Table 2: Variations of I and T (in % with regard to V_1) when considering progressively distant nodes or adding extra nodes. See the **Results** paragraph in the text for the interpretation of pairs and triplets with progressively distant nodes.

generality and relevance of the facts they illustrate (nonlinearities and recurrence) implies that a proper descriptor of functional connectivity should be sensitive to the different variations of the models.

Sections 3.1, 4.2, and 4.3 explicitly show the superiority of T over I in the considered nonlinear and recurrent models. The conclusion of these analytical results (confirmed by the experimental simulations) is that while the conventional *Mutual Information* is not useful to capture the intra-cortical connections in *Model I*, the proposed measure, *Total Correlation*, is quite sensitive to this connectivity. Similarly, the proposed *Total Correlation* is more sensitive than *Mutual Information* to the feedforward and feedback connectivity explored in the recurrent *Model II*. From a general perspective, the considered nonlinearity is ubiquitous in the visual pathway [8, 33, 34, 74, 75]. Therefore, the success of the proposed multivariate *Total Correlation* in describing this connectivity is a substantial advantage with regard to the conventional, pairwise, *Mutual Information*.

Results with real data: T highlights synergies in V_1, V_2, V_3, V_4 . The positive results of T (and the corresponding RBIG estimates) in the analytical settings presented above not only address a limitation of [3], but really justify its use in real scenarios. In the case of fMRI data from the visual regions V_1, V_2, V_3, V_4 , our measurements of T show that: (1) the redundancy within each layer, $T(v_i)$, is reduced along the way, which is consistent with the *Efficient Coding Hypothesis*, (2) the information content measured through $T(v_i, v_i)$ is more stable along the way than the measures given by $I(v_i, v_i)$, particularly if the inner redundancy is discounted. (3) The variation of the pairwise measures of $I(v_i, v_j)$ seems compatible with the *data processing inequality* in a purely feedforward setting $v_1 \rightarrow v_2 \rightarrow v_3 \rightarrow v_4$, however, (4) the multi-node T shows synergies that rule out the purely feedforward scheme. Moreover, it suggests stronger functional connectivity between the nodes V_1, V_2, V_3 than between V_2, V_3, V_4 despite a similar anatomical distance. All this complex behavior is not easy to see just using the conventional I .

Relations with previous work. Firstly, this is the necessary analytical companion of the proposal of *Total Correlation* to measure connectivity [3]. Then, here we have applied this tool to visual areas extending the works that first used *Mutual Information* to assess the connectivity between pairs of visual areas [76] or those that measured *Mutual Information* between V_1 and MT (or V_5) under *Divisive Normalization* transforms [77]. The analysis of *Mutual Information* between progressively deeper visual layers is also related with previous works focused on quantifying the information flow in different nonlinear models of retina- V_1 pathway [10, 11], which were restricted to purely feedforward models.

On the other hand, the approach we took here (quantifying the statistical properties of the responses of real brains or psychophysically plausible models) is related with a body of literature that follows *Barlow's Efficient Coding Hypothesis* in a non-classical direction. Note that the classical direction is *from-statistics-to-biology*: a system optimized for a sensible statistical goal may display biological-like behavior [72, 73]. This is the direction that explained linear receptive fields [18, 31, 32, 63] and sensory nonlinearities [20, 36, 56, 62, 78, 79] from statistics. However, there is literature that reasons in the opposite direction *from-biology-to-statistics*: look at the statistical properties of the responses of biologically plausible systems and you will find statistically interesting behavior. In this regard, redundancy

reduction [21, 37, 80], and efficient information transmission [10, 11, 61, 81] has been found in real and biologically plausible models. And this is similar to the information-theoretic analysis that we did of real and simulated responses.

Limitations and future research. This study has three main limitations that should be addressed by future research. First (and most important) is the limitation of the analytical examples: they addressed fundamental issues such as nonlinearities and recurrence, but they did it in *separate* examples (*Model I* and *Model II*). Moreover, *Model I* didn't include noise after the divisive normalization so that one could apply the property of the variation of T under deterministic transforms, Eq. 8, and the invariance of I under transforms of one of the variables, Eq. 12. Future research should try to get unified expressions for a general nonlinear and recurrent model with noise at all layers.

The second, more instrumental, limitation is related to the specific empirical estimator of T which is necessary in real scenarios. Here we used our *Rotation-Based Iterative Gaussianization* [12, 59], and it proved to follow the trends of the theoretical surfaces in the analytical scenarios. However, RBIG may suffer from errors when the signals are strongly non-Gaussian with multiple modes separated by low probability regions as may happen after Divisive Normalization (see the PDFs of natural images in [11, 21]). An approximate knowledge of the PDF of the signals is required to set the number of iterations in RBIG. Of course, future research can use other empirical estimators as for instance [13–17]. In this regard, the analytical results presented here are a good test-bed for current or future empirical estimators.

Finally, regarding the results with real data, it is important to acknowledge that there are more comprehensive databases. The one we used (*the Algonauts 2021 Challenge* [22]) only considers 1000 videos and has a restricted set of voxels because we wanted a simple proof of concept for our measure T and estimator RBIG on low level regions. The work done here could be extended in different ways. First, the database could be segmented depending on the properties of the stimuli (e.g. color, texture and motion content) because the functional connectivity between the considered regions may depend on these low-level features of the input. This could tell us about the specialization of these regions in different dimensions of the stimuli. Moreover, the computation of connectivity based on T depending on the structure of the scene could clarify the differences in the feedback signals found in figure-ground contexts [69, 71]. And second, larger databases (such as [82]) may be convenient to confirm the current results and be more appropriate to study the connectivity depending on the properties of the input so that the subsets are big enough to trust the information estimates. Databases like [83] can be used to address the relation between V1 and higher-level regions (FFA, PPA,...).

Conclusions: In this work we derived analytical results that show that *Total Correlation* is a better descriptor of connectivity than *Mutual Information* in plausible models of the retina-LGN-V1 that include nonlinearities due to intra-cortical connectivity and top-down feedback. T is better because it is more sensitive than I to connectivity. Analytical results are derived for Gaussian signals but, as confirmed by empirical estimates, they also hold for natural inputs. Our T results for real responses recorded from V1,V2,V3,V4 rule out a naive feedforward-only information flow and suggest stronger feedback connections in V1,V2,V3, than in V2,V3,V4.

The proposed measure opens several possibilities: (1) it can be applied to assess the connectivity in complex models that have been developed to reproduce feedforward and feedback oscillations [70], and (2) it can be used to examine signal-dependent feedback in stimuli with figure-ground or spatially segregated textures, which is an interesting open question in visual neuroscience [69, 71].

6 Author contributions

QL checked the plausibility of the neural models reproducing the psychophysical data, implemented the experiments to compare Total Correlation and Mutual Information, computed the measures in the fMRI data using RBIG and contributed to the writing of the manuscript. GVS made some comments and suggestions on earlier versions of this manuscript, and contributed to the writing of the manuscript. JM had the idea of the work, developed the theoretical results, implemented the neural model, and prepared the first draft of the manuscript.

7 Acknowledgements

The authors thank Dr. Valero Laparra for his comments on early stopping of RBIG depending on data dimensionality and Dr. Olga Stefanska for her support in the writing process. We thank the organizers of the *Algonauts Project 2021 Challenge* for providing their interesting fMRI dataset which was used in this study. This work was partially funded by these spanish/european grants from GVA/AEI/FEDER/EU: MICINN PID2020-118071GB-I00, MICINN PDC2021-121522-C21, and GVA Grisolia-P/2019/035 (for JM and QL), and by the Defense Advanced Research Projects Agency (DARPA) under award FA8750-17-C-0106 (for GVS).

References

- [1] Karl Friston. “Functional and Effective Connectivity: A Review”. In: *Brain connectivity* 1 (Jan. 2011), pp. 13–36.
- [2] J.T. Lizier et al. “Multivariate Information-Theoretic Measures Reveal Directed Information Structure and Task Relevant Changes in fMRI Connectivity”. In: *J. Comput. Neurosci.* 30.1 (2011), pp. 85–107.
- [3] Qiang Li. “Functional connectivity inference from fMRI data using multivariate information measures”. In: *Neural Networks* 146 (2022), pp. 85–97.
- [4] Satoshi Watanabe. “Information theoretical analysis of multivariate correlation”. In: *IBM Journal of research and development* 4.1 (1960), pp. 66–82.
- [5] Thomas M. Cover and Joy A. Thomas. *Elements of Information Theory (Wiley Series in Telecommunications and Signal Processing)*. USA: Wiley-Interscience, 2006. ISBN: 0471241954.
- [6] M. Carandini and D. Heeger. “Summation and Division by Neurons in Visual Cortex”. In: *Science* 264.5163 (1994), pp. 1333–6.
- [7] N.C. Rust and J.A. Movshon. “In praise of artifice”. In: *Nat. Neurosci.* 8 (2005), pp. 1647–1650.
- [8] M. Carandini and D. Heeger. “Normalization as a canonical neural computation”. In: *Nat. Rev. Neurosci.* 13.1 (2012), pp. 51–62.
- [9] M. Martínez, M Bertalmío, and J. Malo. “In Praise of Artifice Reloaded: Caution with Natural Image Databases in Modeling Vision”. In: *Front. Neurosci.* doi: 10.3389/fnins.2019.00008 (2019).
- [10] A. Gomez-Villa, M. Bertalmio, and J. Malo. “Visual Information Flow in Wilson-Cowan Networks”. In: *J. Neurophysiol.* doi:10.1152/jn.00487.2019 (2020).
- [11] J. Malo. “Spatio-chromatic information available from different neural layers via Gaussianization”. In: *J. Math. Neurosci.* 10.18 (2020). DOI: 10.1186/s13408-020-00095-8.
- [12] V. Laparra, G. Camps-Valls, and J. Malo. “Iterative gaussianization: from ICA to random rotations”. In: *IEEE Trans. Neural Networks* 22.4 (2011), pp. 537–549.
- [13] Greg Ver Steeg and Aram Galstyan. “Discovering Structure in High-Dimensional Data Through Correlation Explanation”. In: *Advances in Neural Information Processing Systems, NIPS’14*. 2014.
- [14] Greg Ver Steeg. “Unsupervised Learning via Total Correlation Explanation”. In: *IJCAI*. 2017.
- [15] Greg Ver Steeg and Aram Galstyan. “Maximally Informative Hierarchical Representations of High-Dimensional Data”. In: *AISTATS’15*. 2015.
- [16] Iván Marín-Franch and David H. Foster. “Estimating Information from Image Colors: An Application to Digital Cameras and Natural Scenes”. In: *IEEE Transactions on Pattern Analysis and Machine Intelligence* 35.1 (2013), pp. 78–91.
- [17] Z. Szabó. “Information Theoretical Estimators Toolbox”. In: *Journal of Machine Learning Research* 15 (2014), pp. 283–287.
- [18] Bruno A. Olshausen and David J. Field. “Emergence of simple-cell receptive field properties by learning a sparse code for natural images”. In: *Nature* 381 (1996), pp. 607–609.
- [19] Eero P Simoncelli and Bruno A Olshausen. “Natural Image Statistics and Neural Representation”. In: *Annual Review of Neuroscience* 24.1 (2001), pp. 1193–1216.
- [20] J. Malo and J. Gutiérrez. “V1 non-linear properties emerge from local-to-global non-linear ICA”. In: *Network: Computation in Neural Systems* 17.1 (2006), pp. 85–102.
- [21] J. Malo and V. Laparra. “Psychophysically tuned divisive normalization approximately factorizes the PDF of natural images”. In: *Neural computation* 22.12 (2010), pp. 3179–3206.
- [22] Radoslaw Martin Cichy et al. “The Algonauts Project 2021 Challenge: How the Human Brain Makes Sense of a World in Motion”. In: *CoRR* abs/2104.13714 (2021). arXiv: 2104.13714. URL: <https://arxiv.org/abs/2104.13714>.
- [23] D Cai, Gregory C. DeAngelis, and Ralph D. Freeman. “Spatiotemporal receptive field organization in the lateral geniculate nucleus of cats and kittens.” In: *Journal of neurophysiology* 78 2 (1997), pp. 1045–61.
- [24] Andrew B. Watson. “DCT quantization matrices visually optimized for individual images”. In: *Electronic Imaging*. 1993.
- [25] P.J.B. Hancock, R.J. Baddeley, and L.S. Smith. “The principal components of natural images”. In: *Network* 3 (1992), pp. 61–70.
- [26] Jose Juan Esteve-Taboada et al. “Psychophysical Estimation of Early and Late Noise”. In: *arXiv 10.48550/ARXIV.2012.06608* (2020). URL: <https://arxiv.org/abs/2012.06608>.
- [27] David H Brainard and Spatial Vision. “The psychophysics toolbox”. In: *Spatial vision* 10 (1997), pp. 433–436.

- [28] Eric R. Kandel, James H. Schwartz, and Thomas M. Jessell, eds. *Principles of Neural Science*. Third. New York: Elsevier, 1991.
- [29] Li Zhaoping. “A new framework for understanding vision from the perspective of the primary visual cortex”. In: *Current Opinion in Neurobiology* 58 (2019), pp. 1–10.
- [30] E. Martinez-Uriegas. “Chromatic-achromatic multiplexing in human color vision”. In: ed. by D H Kelly. CRC Press, 1994. Chap. Chapt. 4 in *Visual Science and Engineering: Models and Applications*, pp. 117–187.
- [31] J. Atick, Z. Li, and A. Redlich. “Understanding Retinal Color Coding from First Principles”. In: *Neural Comput.* 4.4 (1992), pp. 559–572.
- [32] Qiang Li et al. “Contrast sensitivity functions in autoencoders”. In: *Journal of Vision* 22.6 (May 2022), pp. 8–8.
- [33] M. Martinez et al. “Derivatives and inverse of cascaded linear+nonlinear neural models”. In: *PLOS ONE* 13.10 (Oct. 2018), pp. 1–49.
- [34] A. B. Watson and J. A. Solomon. “Model of visual contrast gain control and pattern masking”. In: *JOSA A* 14.9 (1997), pp. 2379–2391.
- [35] Rajesh Rao et al. “Natural Image Statistics and Divisive Normalization: Modeling Nonlinearities and Adaptation in Cortical Neurons”. In: *Statistical Theories of the Brain* (Jan. 2001).
- [36] O. Schwartz and E.P. Simoncelli. “Natural signal statistics and sensory gain control”. In: *Nature Neurosci.* 4.8 (2001), pp. 819–825.
- [37] J. Malo and E Simoncelli. “Nonlinear image representation for efficient perceptual coding”. In: *IEEE Trans.Im.Proc.* 15.1 (2006), pp. 68–80.
- [38] Ruben Coen-Cagli, Peter Dayan, and Odelia Schwartz. “Cortical Surround Interactions and Perceptual Saliency via Natural Scene Statistics”. In: *PLOS Comp. Biol.* 8.3 (Mar. 2012), pp. 1–18.
- [39] A. B. Watson and J. Malo. “Video quality measures based on the standard spatial observer”. In: *IEEE Proc. Int. Conf. Im. Proc.* Vol. 3. 2002, pp. III–III.
- [40] J. Malo et al. “Characterization of the human visual system threshold performance by a weighting function in the Gabor domain”. In: *Journal of Modern Optics* 44.1 (1997), pp. 127–148.
- [41] Andrew Watson. “Image Compression Using the DCT”. In: *Mathematica Journal* 4 (Aug. 1994).
- [42] Albert Ahumada and Heidi Peterso. “Luminance-Model-Based DCT Quantization for Color Image Compression”. In: *Proc SPIE Human Vision, Visual Process Display III* 1666 (Dec. 1997).
- [43] Andrew B. Watson, ed. *Digital Images and Human Vision*. Cambridge, MA, USA: MIT Press, 1993. ISBN: 0262231719.
- [44] J. Malo, AM Pons, and J.M. Artigas. “Subjective image fidelity metric based on bit allocation of the human visual system in the DCT domain”. In: *Im. Vis. Comp.* 15.7 (1997), pp. 535–548.
- [45] G. Camps-Valls et al. “Kernel-based Framework for Multi-Temporal and Multi-Source Remote Sensing Data Classification and Change Detection”. In: *IEEE TGRS* 46.6 (2008), pp. 1822–1835.
- [46] Hugh R Wilson and Jack D Cowan. “A mathematical theory of the functional dynamics of cortical and thalamic nervous tissue”. In: *Kybernetik* 13.2 (1973), pp. 55–80.
- [47] Mark A. Georgeson and Timothy S. Meese. “Fixed or variable noise in contrast discrimination? The jury’s still out...” In: *Vision Research* 46.25 (Nov. 2006), pp. 4294–4303.
- [48] M.D. Fairchild. *Color Appearance Models*. The Wiley-IS&T Series in Imaging Science and Technology. Wiley, 2013.
- [49] N. Ponomarenko et al. “Color image database for evaluation of image quality metrics”. In: *2008 IEEE 10th Workshop on Multimedia Signal Processing*. 2008, pp. 403–408.
- [50] V. Laparra, J. Muñoz, and J. Malo. “Divisive normalization image quality metric revisited”. In: *JOSA A* 27.4 (2010), pp. 852–864.
- [51] A. Hepburn et al. “Perceptnet: A Human Visual System Inspired Neural Network For Estimating Perceptual Distance”. In: *IEEE ICIP*. 2020, pp. 121–125.
- [52] P.C. Teo and D.J. Heeger. “Perceptual image distortion”. In: *Proceedings of 1st International Conference on Image Processing*. Vol. 2. 1994, 982–986 vol.2.
- [53] Z. Wang and A. C. Bovik. “Mean squared error: Love it or leave it? A new look at signal fidelity measures”. In: *IEEE Signal Processing Magazine* 26.1 (2009), pp. 98–117.
- [54] Vasily Strela et al. “Adaptive Wiener denoising using a Gaussian scale mixture model in the wavelet domain”. In: *Proceedings 2001 International Conference on Image Processing (Cat. No.01CH37205)* 2 (2001), 37–40 vol.2.
- [55] J. Gutiérrez, F. J Ferri, and J. Malo. “Regularization operators for natural images based on nonlinear perception models”. In: *IEEE Trans. Im. Proc.* 15.1 (2006), pp. 189–200.

- [56] Siwei Lyu and Eero P. Simoncelli. “Nonlinear Extraction of Independent Components of Natural Images Using Radial Gaussianization”. In: *Neural Computation* 21.6 (2009), pp. 1485–1519.
- [57] Alexander Kraskov, Harald Stögbauer, and Peter Grassberger. “Estimating mutual information”. In: *Phys. Rev. E* 69 (6 June 2004), p. 066138.
- [58] Henry Stark and John Woods. *Probability, Random Processes, and Estimation Theory for Engineers*. Vol. 90. Jan. 1994.
- [59] Valero Laparra et al. “Information Theory Measures via Multidimensional Gaussianization”. In: *CoRR* abs/2010.03807 (2020). arXiv: 2010.03807. URL: <https://arxiv.org/abs/2010.03807>.
- [60] J.E. Johnson et al. “Information Theory in Density Destructors”. In: *7th Int. Conf. Mach. Learn., ICML 2019, Workshop on Invertible Normalization Flows*. 2019.
- [61] Jesús Malo. “Information flow in Color Appearance Neural Networks”. In: *Proceedings of Entropy 2021: The Scientific Tool of the 21st Century* (2019).
- [62] V. Laparra et al. “Nonlinearities and adaptation of color vision from sequential principal curves analysis”. In: *Neural Computation* 24.10 (2012), pp. 2751–2788.
- [63] M. U Gutmann et al. “Spatio-chromatic adaptation via higher-order canonical correlation analysis of natural images”. In: *PloS one* 9.2 (2014), e86481.
- [64] J. Vazquez-Corral et al. “Color Constancy Algorithms: Psychophysical Evaluation on a New Dataset”. In: *Journal of Imaging Science and Technology* 53.3 (2009), pp. 31105-1-31105–9.
- [65] I. Epifanio, J. Gutierrez, and J. Malo. “Linear transform for simultaneous diagonalization of covariance and perceptual metric matrix in image coding”. In: *Patt. Recog.* 36.8 (2003), pp. 1799–1811.
- [66] R.J. Clarke. “Relation between the Karhunen Loève and cosine transforms”. In: *IEE Proceedings F (Comm. Radar Sig. Proc.)* 128 (6 1981), pp. 359–361.
- [67] João Semedo et al. “Feedforward and feedback interactions between visual cortical areas use different population activity patterns”. In: *Nat Commun* 1099 (2022), p. 13.
- [68] Timo van Kerkoerle et al. “Alpha and gamma oscillations characterize feedback and feedforward processing in monkey visual cortex”. In: *PNAS* 111.40 (2014), pp. 14332–14341.
- [69] P. Christiaan Klink et al. “Distinct Feedforward and Feedback Effects of Microstimulation in Visual Cortex Reveal Neural Mechanisms of Texture Segregation”. In: *Neuron* 95.1 (2017), 209–220.e3.
- [70] Jorge F. Mejias et al. “Feedforward and feedback frequency-dependent interactions in a large-scale laminar network of the primate cortex”. In: *Science Advances* 2.11 (2016), e1601335.
- [71] Hulusi Kafaligonul, Bruno Breitmeyer, and Haluk Ögmen. “Feedforward and feedback processes in vision”. In: *Front. Psychol.* 6 (Mar. 2015).
- [72] H. Barlow. “Possible Principles Underlying the Transformations of Sensory Messages”. In: *Sensory Comm.* 1 (Jan. 1961).
- [73] H. Barlow. “Redundancy reduction revisited”. In: *Network: Comp. Neur. Syst.* 12.3 (2001), pp. 241–253.
- [74] J. M. Hillis and D.H. Brainard. “Do common mechanisms of adaptation mediate color discrimination and appearance?” In: *JOSA A* 22.10 (2005), pp. 2090–2106.
- [75] E. Simoncelli and D. Heeger. “A model of neuronal responses in visual area MT”. In: *Vis. Res.* 38.5 (1998), pp. 743–761.
- [76] B. Chai et al. “Exploring Functional Connectivities of the Human Brain using Multivariate Information Analysis”. In: *NIPS*. Ed. by Y. Bengio. Vol. 22. Curran Associates, Inc., 2009, pp. 270–278.
- [77] Sameer Saproo and John T. Serences. “Attention Improves Transfer of Motion Information between V1 and MT”. In: *J. Neurosci.* 34.10 (2014), pp. 3586–3596.
- [78] T.v.d. Twer and D.I.A. MacLeod. “Optimal nonlinear codes for the perception of natural colours”. In: *Network: Computation in Neural Systems* 12.3 (2001), pp. 395–407.
- [79] V. Laparra and J. Malo. “Visual aftereffects and sensory nonlinearities from a single statistical framework”. In: *Front. Human Neurosci.* 9 (2015), p. 557.
- [80] A. Renart et al. “The asynchronous state in cortical circuits”. In: *Science* 327(5965) (2010), pp. 587–590.
- [81] D.H. Foster, I. Marin-Franch, and S.M.C. Nascimento. “Coding efficiency of CIE color spaces”. In: *Proc. 16th Color Imag. Conf. Soc. Imag. Sci. Tech.* 2008, pp. 285–288.
- [82] E.J. Allen, G. St-Yves, and Y. Wu. “A massive 7T fMRI dataset to bridge cognitive neuroscience and artificial intelligence.” In: *Nature Neurosci.* 25 (2022), pp. 116–126.
- [83] N. Chang, J.A. Pyles, and A. Marcus. “BOLD5000, a public fMRI dataset while viewing 5000 visual images.” In: *Sci. Data* 6 (2019), p. 49.